

# BRAIN COMMUNICATIONS

## Axon hyperexcitability in the contralateral projection following unilateral optic nerve crush in mice

Nolan R. McGrady,<sup>1</sup> Joseph M. Holden,<sup>1</sup> Marcio Ribeiro,<sup>1</sup> Andrew M. Boal,<sup>1</sup> Michael L. Risner<sup>1</sup> and David J. Calkins<sup>1</sup>

Optic neuropathies are characterized by degeneration of retinal ganglion cell axonal projections to the brain, including acute conditions like optic nerve trauma and progressive conditions such as glaucoma. Despite different aetiologies, retinal ganglion cell axon degeneration in traumatic optic neuropathy and glaucoma share common pathological signatures. We compared how early pathogenesis of optic nerve trauma and glaucoma influence axon function in the mouse optic projection. We assessed pathology by measuring anterograde axonal transport from retina to superior colliculus, current-evoked optic nerve compound action potential and retinal ganglion cell density 1 week following unilateral optic nerve crush or intraocular pressure elevation. Nerve crush reduced axon transport, compound axon potential and retinal ganglion cell density, which were unaffected by intraocular pressure elevation. Surprisingly, optic nerves contralateral to crush demonstrated 5-fold enhanced excitability in compound action potential compared with naïve nerves. Enhanced excitability in contralateral sham nerves is not due to increased accumulation of voltage-gated sodium channel 1.6, or ectopic voltage-gated sodium channel 1.2 expression within nodes of Ranvier. Our results indicate hyperexcitability is driven by intrinsic responses of  $\alpha$ ON-sustained retinal ganglion cells. We found  $\alpha$ ON-sustained retinal ganglion cells in contralateral, sham and eyes demonstrated increased responses to depolarizing currents compared with those from naïve eyes, while light-driven responses remained intact. Dendritic arbours of  $\alpha$ ON-sustained retinal ganglion cells of the sham eye were like naïve, but soma area and non-phosphorylated neurofilament H increased. Current- and light-evoked responses of sham  $\alpha$ OFF-sustained retinal ganglion cells remained stable along with somato-dendritic morphologies. In retinas directly affected by crush, light responses of  $\alpha$ ON- and  $\alpha$ OFF-sustained retinal ganglion cells diminished compared with naïve cells along with decreased dendritic field area or branch points. Like light responses,  $\alpha$ OFF-sustained retinal ganglion cell current-evoked responses diminished, but surprisingly,  $\alpha$ ON-sustained retinal ganglion cell responses were similar to those from naïve retinas. Optic nerve crush reduced dendritic length and area in  $\alpha$ ON-sustained retinal ganglion cells in eyes ipsilateral to injury, while crush significantly reduced dendritic branching in  $\alpha$ OFF-sustained retinal ganglion cells. Interestingly, 1 week of intraocular pressure elevation only affected  $\alpha$ OFF-sustained retinal ganglion cell physiology, depolarizing resting membrane potential in cells of affected eyes and blunting current-evoked responses in cells of saline-injected eyes. Collectively, our results suggest that neither saline nor sham surgery provide a true control, chronic versus acute optic neuropathies differentially affect retinal ganglion cells composing the ON and OFF pathways, and acute stress can have near-term effects on the contralateral projection.

1 Department of Ophthalmology and Visual Sciences, Vanderbilt Eye Institute, Vanderbilt University Medical Center, AA7103 MCN/VUIIS, 1161 21st Ave. S., Nashville, TN 37232, USA

Correspondence to: David J. Calkins, PhD  
AA7103 MCN/VUIIS 1161  
21st Ave. S., Nashville, TN 37232, USA  
E-mail: david.j.calkins@vumc.org

Received March 16, 2022. Revised August 02, 2022. Accepted October 01, 2022. Advance access publication October 3, 2022

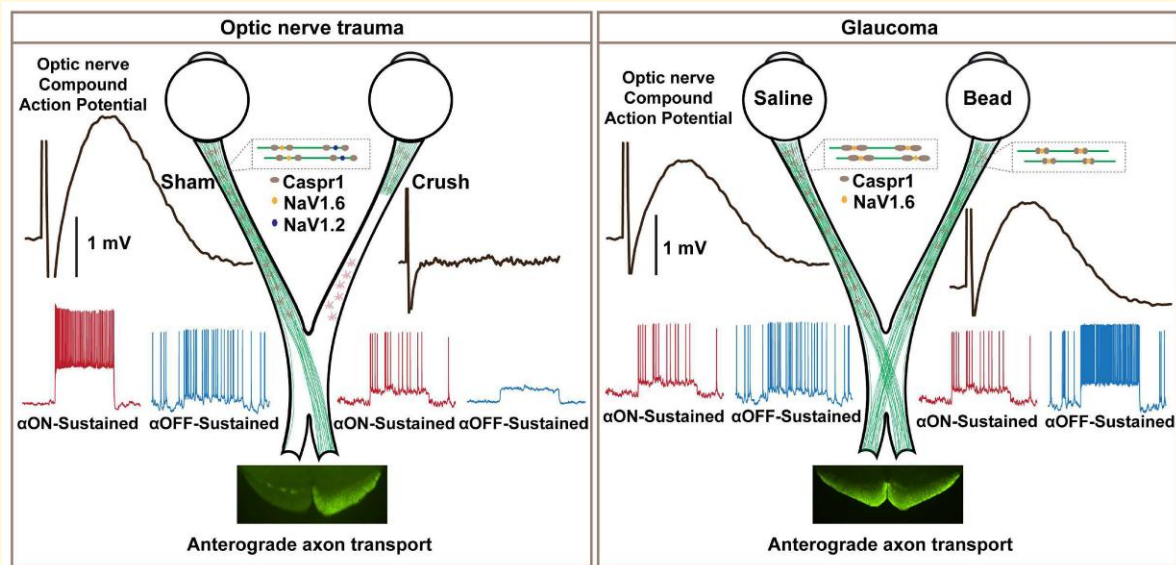
© The Author(s) 2022. Published by Oxford University Press on behalf of the Guarantors of Brain.

This is an Open Access article distributed under the terms of the Creative Commons Attribution License (<https://creativecommons.org/licenses/by/4.0/>), which permits unrestricted reuse, distribution, and reproduction in any medium, provided the original work is properly cited.

**Keywords:** traumatic optic neuropathy; glaucoma; retinal ganglion cells; hyperexcitability; degeneration

**Abbreviations:** CTB=cholera toxin subunit B; GFAP=glial fibrillary acidic protein; IOP=intraocular pressure; NaV=voltage-gated sodium channel; ONC=optic nerve crush; RMP=resting membrane potential; RGC=retinal ganglion cell; SC=superior colliculus; SMI-32=non-phosphorylated neurofilament H.

## Graphical Abstract



## Introduction

Tissue damage caused by neurodegenerative diseases and acute conditions is often regionally confined during early progression. Over time, however, degeneration can spread secondarily to surrounding regions. For example, clinical and experimental evidence indicate ischaemic stroke initially affects a central core. Neighbouring tissues then react, redistributing resources to restore homeostasis to the core at the expense of depleting local reserves, which effectively increases the infarct area.<sup>1,2</sup> Similarly, glaucomatous optic neuropathy (glaucoma) initially attacks select retinal ganglion cell (RGC) axons that compose the superior and inferior poles of the optic nerve, causing deficits in mid-peripheral visual fields.<sup>3</sup> Visual field deficits gradually expand along with increased RGC axon degeneration.<sup>4</sup> Typically, glaucoma occurs bilaterally but often develops asymmetrically where the eye dominated by disease progresses more rapidly than the contralateral eye.<sup>5</sup> This asymmetrical loss in visual field sectors appears to be directed by central mechanisms to maintain intact binocular fields.<sup>6</sup> This clinical evidence suggest nerve damage spreads locally within and between optic projections, and retrograde signals direct compensatory mechanisms to maintain function. Similarly, in experimental glaucoma, unilateral intraocular pressure (IOP) elevation and optic nerve stress activate astrocytes and innate immune cells in the contralateral retina and projection.<sup>7,8,9,10,11,12</sup> Although the contralateral retina and projection indicate a pro-inflammatory

response during unilateral IOP elevation, the overall RGC activity remains intact.<sup>10</sup> Even short-term unilateral IOP elevation produces a compensatory responses where astrocytes of the contralateral nerve donate metabolic resources to the stressed nerve, rendering the uninjured nerve susceptible to degeneration when subsequently stressed.<sup>13</sup> Modelling traumatic insult, unilateral optic nerve crush (7–9 days) downregulates the RGC-specific transcription factor Brn3a, upregulates caspase-3, significantly reduces RGC density in the contralateral retina, though central neuron density remains stable.<sup>7–14</sup> This line of evidence indicates stress is not limited to the projection directly affected and distal structures may persist during degeneration.<sup>15</sup>

Here, we sought to compare the pathophysiology of murine RGCs and their axons in directly injured versus contralateral tissues following optic nerve crush or induced IOP elevation by injection of microbeads.<sup>16</sup> We examined RGC axon transport to the superior colliculus (SC), excitatory signalling in the optic nerve assessed through compound action potential, and RGC light- and current-evoked responses and dendritic arbour morphology. Optic nerve crush significantly reduced RGC dendritic complexity, impaired axon transport and diminished the compound action potential in the affected nerve compared with IOP elevation. Overall, we found both optic nerve crush and IOP elevation affected tissues of the contralateral projection compared with naïve. Interestingly, optic nerve crush increased excitability in the contralateral sham nerve, despite reduced expression of

voltage-gated Na<sup>+</sup> (NaV) channel isoform NaV1.6. We also observed contralateral hyperexcitability in large-field RGCs that produce a sustained response to light increments (i.e.  $\alpha$ ON-sustained RGCs) but not in RGCs signalling light offset ( $\alpha$ OFF-sustained RGCs). Based on our results from light- and current-evoked responses of  $\alpha$ ON-sustained RGCs, hyperexcitability appears independent of pre-synaptic mechanisms. These results suggest unilateral optic nerve crush piques mechanisms in the contralateral nerve that retrogradely influence voltage-gated activity in  $\alpha$ ON-sustained RGCs.

## Materials and methods

### Animals

All animal experiments described herein were approved by the Vanderbilt University Institutional Animal Care and Use Committee. We obtained adult (1.5–2 months old) male ( $n=40$ ) and female ( $n=15$ ) C57Bl/6 mice from Charles River Laboratories (Wilmington, MA, USA). Mice were housed at the Vanderbilt Division of Animal Care on a 12 h light/dark cycle and provided water and standard rodent chow as desired.

### IOP elevation and optic nerve crush

We measured IOP using TonoPen XL (Reichert Technologies, Depew, NY, USA), which was designed for use on human eyes. Previous studies indicate IOP measurements obtained from rodents using TonoPen correlate with direct cannulation measurements but requires a correction.<sup>17,18</sup> We included corrected IOP measurements using the appropriate regression relationship between direct cannulation and Tonopen values from a previous study with cannulated IOP measurements.<sup>18</sup> Additionally, our laboratory has shown reproducible IOP measurements from rodents with the TonoPen XL across many users, in line with the values we report here.<sup>15–19,20,21,22,23,24,25</sup>

TonoPen XL was calibrated each day prior to measuring IOPs according to the manufacturer's specifications. The Ocu-Film cover (230651; Reichert Technologies) was used during measurements. Prior to performing IOP measurements, mice were anaesthetized (2.5% isoflurane). We recorded IOP of naïve eyes (baseline) on 2 separate days. We defined baseline IOP as the average of the two measurements of naïve eyes (Day 0). Following baseline IOP measurements, we unilaterally elevated IOP by injecting 1.5  $\mu$ l of 15  $\mu$ m polystyrene microbeads (Invitrogen, Carlsbad, CA, USA) into the anterior chamber; the fellow eye received an equal volume of sterile saline to serve as the control. We measured IOP two to three times per week for 1 week as described previously.<sup>13–21,22,23–25,26,27</sup>

We performed unilateral optic crush in anaesthetized [ketamine (112 mg/kg, KetaVed; Vedco Inc., St Louis, MO, USA)/xylazine (7 mg/kg, AnaSed injection; Akorn Inc., Lake Forest,

IL, USA)] C57Bl/6 mice. After sedation, we provided analgesia through intraperitoneal injection of ketoprofen (5 mg/kg, Ketofen; Zoetis Inc., Parsippany, NJ, USA). The optic nerve was exposed by performing a lateral canthotomy followed by a small incision in the conjunctiva. Afterwards, we used self-closing forceps (RS-5020; Roboz Surgical Instrument Co., Gaithersburg, MD, USA) to crush the optic nerve ~1 mm posterior to the globe for 10 s. The contralateral nerve was also exposed but was not crushed. Afterwards, we applied triple antibiotic ointment (22373; Medique Products, Fort Myers, FL, USA) to the surgical site, and we monitored mice during their recovery from anaesthesia. Mice were kept on a heating pad both during surgery and while recovering to preserve body temperature.

### Anterograde axonal transport

We determined the fidelity of anterograde transport of RGC axons to their target neurons in the SC by measuring the transfer of cholera toxin subunit B (CTB) conjugated to Alexa Fluor 488 (CTB; Molecular Probes, Eugene, OR, USA). We intravitreally injected 1.5  $\mu$ l of 1  $\mu$ g/ $\mu$ l solution of CTB using a Hamilton syringe (7643-01; Hamilton, Reno, NV, USA) in anaesthetized mice (2.5% isoflurane). Two days after CTB injection, we transcardially perfused mice as described earlier.<sup>15–19,20,21–25</sup> Following perfusion, we dissected out brains and cryoprotected in 20% sucrose solution. We then obtained coronal midbrain sections (50  $\mu$ m) using a freezing sliding microtome (SM2000R; Leica Biosystems, Buffalo Grove, IL, USA). We imaged CTB fluorescence in alternating sections of the SC using a Nikon Ti Eclipse microscope. We quantified CTB signal intensity using a custom ImagePro (ImagePro 7; Media Cybernetics, Rockville, MD, USA) macro as described previously.<sup>15</sup>

### Optic nerve physiology

We measured mouse optic nerve compound action potentials using methods previously developed in our laboratory.<sup>13–24</sup> We euthanized animals by cervical dislocation and decapitation. Afterwards, the top of the skull was removed, and we gently tilted the brain upward to expose the optic nerves. We severed optic nerves at the optic chiasm and posterior to the optic nerve head. Once detached, we immediately placed optic nerves in ice-cold (4°C) carbogen-saturated (95% O<sub>2</sub>, 5% CO<sub>2</sub>) artificial cerebrospinal fluid (aCSF) for 30 min. The aCSF contained (in mM) 124 NaCl, 3 KCl, 2 CaCl<sub>2</sub>, 2 MgCl<sub>2</sub>, 1.25 NaH<sub>2</sub>PO<sub>4</sub>, 23 NaHCO<sub>3</sub> and 10 glucose.<sup>28</sup> The pH of the aCSF was 7.4. Optic nerves were equilibrated to physiological conditions for 30 min prior to recording. To prevent any order effects, we alternated the order we performed physiology on optic nerves.

We transferred optic nerves singly using a paint brush into a physiological recording chamber (Model PH1; Warner Instruments, Holliston, MA, USA) and continually perfused carbogen-saturated aCSF at a rate of 2 mL/min using a

peristaltic pump (Model 7518; Masterflex, Vernon Hills, IL, USA). We maintained the aCSF solution at 35°C (Model TC-344C; Warner Instruments). The caudal end of the optic nerve was positioned into a recording suction electrode (Model 573040; A-M Systems, Sequim, WA, USA), and the rostral end of the optic nerve was positioned into a custom-made stimulating suction electrode. We fabricated electrodes with an average 350  $\mu\text{m}$  diameter bore from borosilicate glass (Model TW150-4; WPI, Sarasota, FL, USA) using a puller system (Model P2000; Sutter Instruments, Novato, CA, USA). Recording and stimulating electrodes were fixed to separate micromanipulators (Model MM33; WPI). The stimulating electrode contained an Ag wire, and the recording pipette contained an Ag/AgCl<sup>-</sup> wire; we filled both pipettes with aCSF. Optic nerves were stimulated (Model ISO-STIM 01-DPI; NPI Electronic, Germany) and evoked potentials were bandpass filtered (0.0001–10 kHz), amplified (100 $\times$  gain, EXT-02-B; NPI Electronic), digitized (Digidata 1440A; Molecular Devices, San Jose, CA, USA) and sampled at 50 kHz (Clampex 10.6; Molecular Devices). Resistance between the nerve and recording pipette was measured by an electrode resistance meter (Model REL-08 B; NPI Electronic).

## RGC physiology

We performed whole-cell recordings from whole-mount mouse retinas as previously described.<sup>19–27</sup> Animals were euthanized by cervical dislocation, eyes were enucleated, and retinas were dissected out under long-wavelength illumination (630 nm, 800  $\mu\text{W}/\text{cm}^2$ , FND/FG; Ushio, Cypress, CA, USA). Retinas were placed in carbogen-saturated Ames' medium (US Biologic, Memphis, TN, USA) containing 20 mM glucose and 22.6 mM NaHCO<sub>3</sub> (pH 7.4, 290 Osm). Retinas were mounted onto a physiological chamber, perfused with Ames' medium at a rate of 2 ml/min and maintained at 35°C (Model TC-344C; Warner Instruments).

Retinal ganglion cells were visualized with an Andor CCD camera attached to an Olympus BX50 upright microscope using a 40 $\times$  objective. For intracellular recordings, pipettes were constructed from borosilicate glass (Sutter Instruments) and filled with (in mM): 125 K-gluconate, 10 KCl, 10 HEPES (4-(2-hydroxyethyl)-1-piperazineethanesulfonic acid), 10 EGTA (ethyleneglycol-bis( $\beta$ -aminoethyl)-N,N,N',N'-tetraacetic acid), 4 Mg-ATP, 1 Na-GTP (guanosine triphosphate) and 0.1 ALEXA 555 (Invitrogen). The pH of the intracellular solution was 7.35 and the osmolarity was 285 Osm. Resistances of pipettes containing intracellular solution were between 4 and 8 M $\Omega$ . Whole-cell signals were amplified (Multiclamp 700B; Molecular Devices) and digitized at a sampling rate of 50 kHz (Digidata 1550A; Molecular Devices). In a typical experiment, we measured resting membrane potential (RMP), light-evoked spike activity (full-field 365 nm, 3 s duration, pE-4000; CoolLED, Andover, UK) and voltage-gated responses to depolarizing current injections.

Following completion of physiology experiments, retinas were fixed in 4% paraformaldehyde (PFA) for 24 h at 4°C.

## RGC immunohistochemistry and dendritic arbour analysis

After overnight fixation, retinas were immunolabelled for non-phosphorylated neurofilament H (SMI-32, 1:1000; BioLegend, San Diego, CA, USA) and choline acetyltransferase (ChAT, 1:500; Millipore, Burlington, MA, USA). Retinas were incubated in a blocking solution with 5% normal donkey serum for 2 h and then incubated for 3 days at 4°C with primary antibodies. We imaged RGCs *en montage* using an Olympus FV1000 inverted confocal microscope. RGC dendritic morphologies were hand traced in Adobe Photoshop, and we measured cross-sectional soma area, dendritic area, total dendritic length and number of branching points.<sup>19,21–23</sup> The total dendritic length was defined as the sum of all dendritic lengths. A branch point was defined as the point of bifurcation of a dendrite from a parent dendrite. We also determined dendritic complexity using Sholl analysis (ImageJ version 1.53c), which measures the number of dendritic intersections with 10  $\mu\text{m}$  concentric circles extending from the soma to distal dendritic tips ( $\sim$ 300  $\mu\text{m}$ ).

In a separate set of experiments, after IOP elevation or optic nerve crush, mice were transcardially perfused with phosphate-buffered saline (PBS) followed by 4% PFA. Whole retinas were dissected out and further post fixed in 4% PFA for 2 h at room temperature. We washed retinas 3 $\times$  in PBS and incubated in blocking solution with 5% normal donkey serum. Retinas were incubated for 3 days at 4°C with the RGC selective marker RNA-binding protein with multiple splicing (1:200; PhosphoSolutions, Aurora, CO, USA) followed by incubation with secondary antibody for 2 h at room temperature. Whole retinas were imaged with a Nikon Ti Eclipse microscope (Nikon Instruments Inc., Melville, NY, USA) by a masked investigator. At least eight areas of each retina were used for cell counting. All cell counts were performed by a masked investigator.

## Optic nerve immunohistochemistry and node of Ranvier analysis

Mice were transcardially perfused with PBS and 4% PFA. Full-length optic nerves (from globe to optic chiasm) were then dissected. Optic nerves were post fixed in 4% PFA for 2 h, washed in PBS and then transferred to 30% sucrose for 3 days at 4°C. Optic nerves were placed in optimal cutting temperature medium and cryo-sectioned longitudinally. Nerve sections were washed 3 $\times$  in PBS and then incubated in blocking solution containing 5% normal donkey serum for 2 h at room temperature. To visualize the crush site, optic nerve sections from CTB injected mice were incubated with glial fibrillary acidic protein (GFAP; 1:500; Abcam, Cambridge, UK) and counterstained with DAPI. Sections were incubated overnight at 4°C with primary antibodies Caspr1 (1:300; Millipore, Norwood, OH, USA), NaV1.6

(1:200; Millipore, Norwood, OH, USA) or NaV1.2 (1:300; Alomone Labs, Israel) followed by incubation with appropriate secondary antibodies for 2 h at room temperature. We verified NaV1.6 and NaV1.2 immunolabelling by preabsorbing tissue in blocking peptides prior to adding primary antibodies. Following immunohistochemical procedures, images were captured on an Olympus FV1000 confocal microscope using a 100 $\times$  objective with a 2 $\times$  zoom.

To analyse nodes of Ranvier, linear-segmented regions of interest (ROIs) were traced across the length of both paranodes in an individual axon segment as indicated by Caspr1 staining using ImageJ and ROIs were saved. The ROIs were then accessed by a Python script and ROI pixel values from corresponding NaV1.6 and Caspr1 channels were used to determine critical points (maxima, minima and region bounds). When plotted, Caspr1 shows a roughly bimodal distribution with maxima corresponding to the paranode region and minima corresponding to the node region. NaV1.6 staining shows a complementary pattern with a single maximum in the node region. A threshold was used to determine the boundaries of the node and paranode. Plots were generated for both the Caspr1 and NaV1.6 channels, critical points and the threshold line. These plots were manually checked for quality control, and low-quality plots were removed from the data prior to analysis. We measured the presence or absence of NaV1.2 labelling to determine the percent of NaV1.2-positive nodes quantified.

## Statistical analysis

We analysed and graphed data using Graphpad Prism (Version 9; Graphpad LLC, San Diego, CA, USA). Prior to quantification, we performed outlier (Grubb's test) and normality tests (D'Agostino and Pearson test). For normally distributed data ( $\alpha=0.05$ ), we performed parametric statistics (e.g. one-way ANOVA, *t*-test). If data sets failed normality tests, we performed non-parametric statistics (e.g. Kruskal–Wallis, Mann–Whitney). We identify the statistical test used for each analysis in the figure legends.

## Data availability

Data is available upon reasonable request from the corresponding author.

## Results

### Optic nerve crush increases axon excitability in the contralateral nerve

Here, we compared pathology of RGCs and their axons using two models of optic neuropathy: the microbead occlusion model of glaucoma and optic nerve crush (i.e. traumatic optic neuropathy). For mice in the glaucoma cohort, we found TonoPen-measured IOP increased 1 day post-unilateral injection of microbeads and remained

elevated for the duration of the experiment (+29.5%,  $P < 0.001$ , Fig. 1A, left). IOP of the affected eye significantly increased by 30.7% compared with saline-injected eyes ( $20.76 \pm 1.09$  versus  $15.89 \pm 0.76$  mmHg,  $P = 0.005$ , Fig. 1A, right). When the mean values are corrected using a regression based on a published comparison with cannulation measurements for mice,<sup>18</sup> the relative elevation in IOP increased to 51% (21.8 versus 14.4 mmHg). Despite these elevations in IOP, we did not detect RGC body dropout when compared with saline-injected eyes ( $P > 0.99$ , Supplementary Fig. 1). For animals in the traumatic optic neuropathy cohort, we confirmed injury site in longitudinal nerve sections by immunolabelling against GFAP, counterstaining nuclei with DAPI and tracking RGC active uptake and anterograde transport of CTB (Fig. 1B). Seven days post-unilateral optic nerve crush, we identified the injury site by the absence of GFAP labelling, aggregate DAPI-positive nuclei and loss of CTB transport by RGC axons. Degeneration caused by optic nerve crush was further evidenced by a significant loss of RGC bodies ( $P = 0.04$ , Supplementary Fig. 1). The contralateral eye, receiving sham surgery, appeared to maintain intact axons and RGC density (Fig. 1B, Supplementary Fig. 1).

We determined the influence of glaucoma or traumatic optic neuropathy on axon metabolic and electrical function by measuring RGC anterograde axonal transport of CTB to the SC and optic nerve compound action potential, respectively. After 1 week, axonal transport appeared intact in mice receiving saline and microbead injections, as well as in the sham surgery group (Fig. 1C). Optic nerve crush significantly reduced anterograde axonal transport of CTB to the SC by 78% compared with sham ( $P < 0.001$ , Fig. 1C and D).

Intact optic nerves produced a single peak in response to depolarizing current stimulation (Fig. 1E, left). We did not detect a significant difference between optic nerve compound action potentials of male and female mice (contralateral:  $P > 0.99$ , crush:  $P > 0.99$ ). Therefore, we pooled these data. We found compound action potentials from nerves originating from saline-injected eyes similar to naïve nerves ( $3.14 \pm 0.6$  versus  $5.57 \pm 0.20$  mV,  $P = 0.755$ , Fig. 1E, left, F).<sup>24</sup> Following 1 week of IOP elevation, optic nerve compound action potential remained similar to that of saline-injected eyes ( $2.84 \pm 0.31$  versus  $3.14 \pm 0.6$  mV,  $P > 0.99$ , Fig. 1E, left, F). However, this depolarizing response appeared to be eradicated following crush (Fig. 1E, right). Indeed, optic nerve crush significantly reduced compound action potentials ( $0.27 \pm 0.13$  mV) compared with potentials evoked from naïve (−95%,  $P = 0.006$ ) and sham nerves (−98%,  $P < 0.001$ , Fig. 1E and F). Interestingly, we found the optic nerve compound action potential of the sham nerve increased by 170–377% compared with naïve and saline, respectively ( $P < 0.001$ , Fig. 1F).

Action potential regeneration is dependent on NaV channels accumulating within the nodes of Ranvier. Within mature nodes of Ranvier, NaV subunit 1.6 (NaV1.6) is the dominant isoform.<sup>29</sup> Evidence suggest NaV1.6-mediated hyperexcitability is a subclinical indicator of neurodegenerative

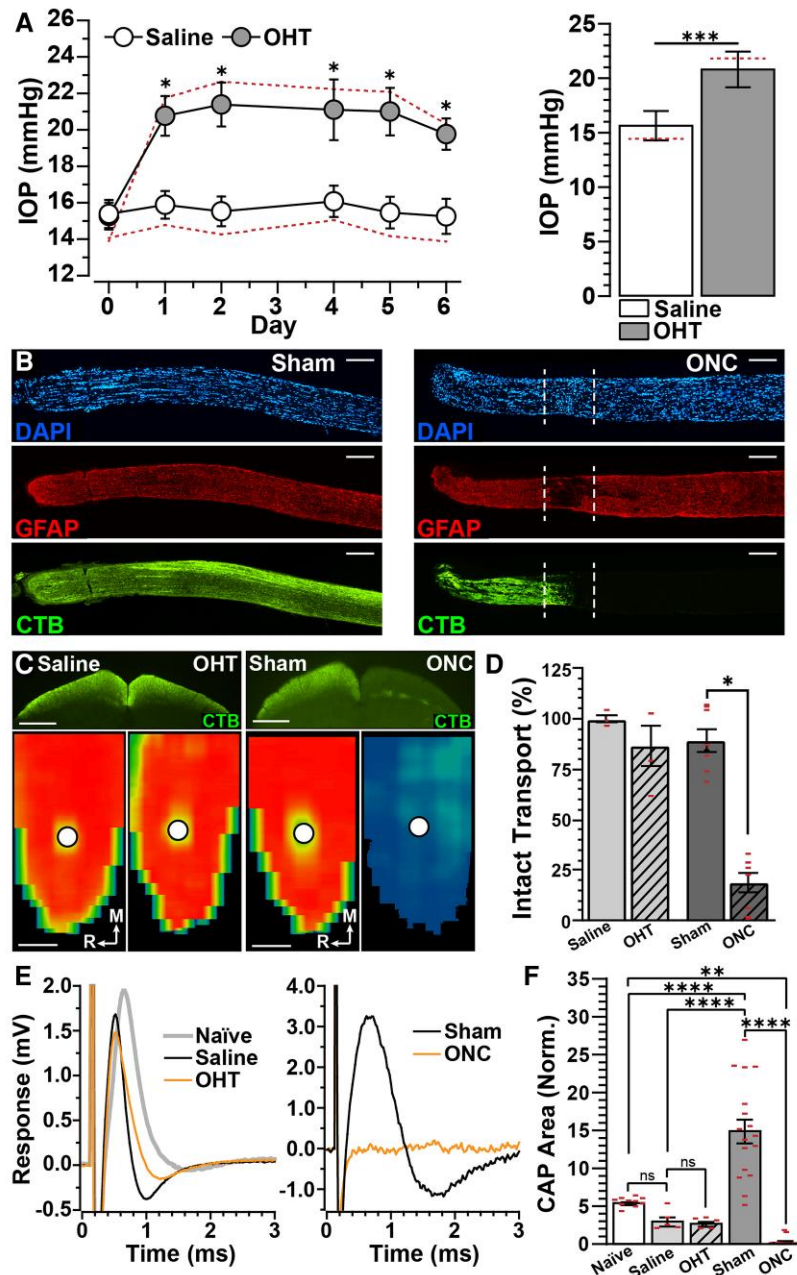


**Figure 1** Unilateral crush induces axonal hyperexcitability in the contralateral nerve. **(A, left)** IOP elevation following a single unilateral injection of polystyrene microbeads ( $1.5 \mu\text{l}$ ,  $n = 14$ ) or saline ( $1.5 \mu\text{l}$ ,  $n = 14$ ;  $P < 0.05$ ). **(A, right)** Mean IOP is elevated by 31% in microbead-injected eyes compared with saline controls ( $P < 0.001$ ). Mean IOP corrected from a published regression based on cannulation measurements (red dotted line, see Reitsamer et al.<sup>18</sup>) resulted in a 5% increase in microbead IOPs and an 8% decrease in saline compared with our TonoPen XL measurements. **(B)** Longitudinal optic nerve sections immunolabelled for GFAP (middle panels) and counterstained with DAPI (blue) in (left) sham and (right) crush nerves. Intact CTB tracing indicates robust anterograde transport in sham nerves. In crushed nerves, deficits in CTB fluorescence indicates injury site (dashed lines). Scale bar = 200  $\mu\text{m}$ . **(C)** CTB transport (top panels) to the SC and corresponding intensity heat maps (bottom) following (left) microbead injection and (right) ONC. Circles indicate optic discs. Scale bar = 500  $\mu\text{m}$ . **(D)** Percentage of intact CTB transport to the SC is similar between eyes subjected to ocular hypertension (OHT) and saline injection ( $P = 0.55$ ,  $n = 4$ ). Transport is significantly diminished 1 week (1Wk) post ONC compared with sham controls ( $P < 0.0001$ ,  $n = 8$ ). **(E)** Representative current-evoked optic nerve compound action potential (CAP) traces from (left) naïve, saline, 1Wk OHT, (right) sham and 1Wk ONC. **(F)** Optic nerve CAP responses of naïve, saline and 1Wk OHT were statistically similar ( $P \geq 0.67$ ,  $n \geq 5$ ). ONC significantly reduced CAP responses compared with naïve ( $P = 0.007$ ,  $n \geq 10$ ) and sham nerves ( $P < 0.0001$ ,  $n = 17$ ). Sham optic nerve CAP responses dramatically increased compared with naïve ( $P < 0.0001$ ,  $n \geq 10$ ) and saline optic nerves ( $P < 0.0001$ ,  $n \geq 4$ ). We normalized optic nerve CAP area to recording pipette resistance. Statistics: **(A)** Unpaired *t*-test. **(D and F)** One-way ANOVA and Tukey's *post hoc* test. Significance indicators: \* $< 0.05$ , \*\* $< 0.01$ , \*\*\* $< 0.001$ , \*\*\*\* $< 0.0001$ . Data are presented as mean  $\pm$  SEM.

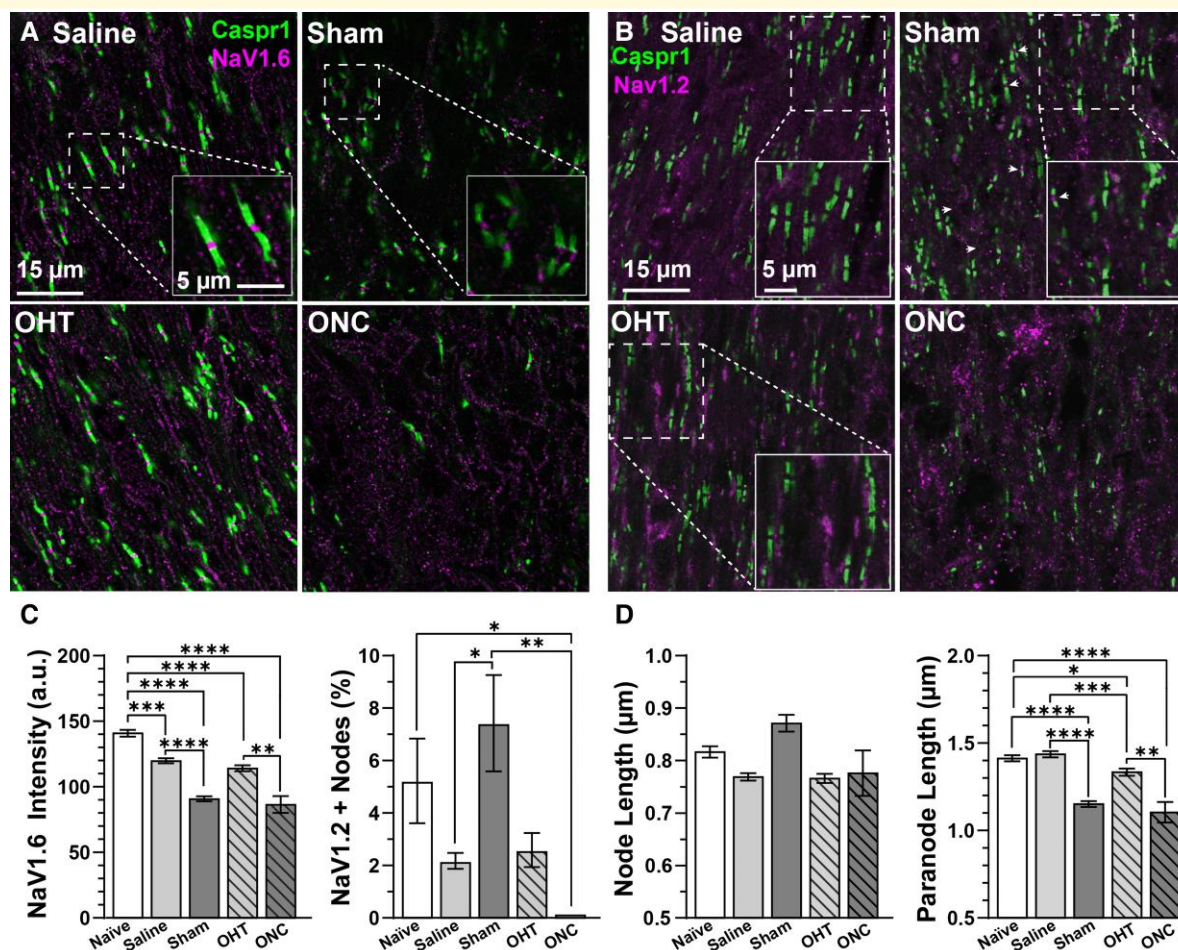


**Figure 2** Reduced expression of NaV1.6 and paranode morphology in experimental nerves. Confocal micrographs of longitudinal optic nerve sections in subject to saline- and microbead injection or sham surgery and ONC. **(A)** Immunostaining of Caspr1-labelled paranodes and NaV1.6 within nodes of Ranvier (scale bar = 15 µm). Insets are higher magnification micrographs showing example node-paranode complexes (scale bar = 5 µm). **(B)** Immunostaining of Caspr1-labelled paranodes and Nav1.2 (scale bar = 15 µm). Insets are higher magnification micrographs showing representative node-paranode complexes (scale bar = 5 µm). **(C, left)** Compared with nerves from naïve mice, NaV1.6 immunolabelling decreased in nerves from all experimental animals ( $P < 0.008$ ,  $n \geq 592$  nodes,  $n \geq 3$  animals). After 1Wk ONC, NaV1.6 intensity also significantly diminished compared with optic nerves from 1Wk OHT mice ( $P = 0.0027$ ,  $n \geq 49$ ,  $n \geq 3$  animals). **(C, right)** We did not detect a significant difference in NaV1.2 expression between naïve, saline, sham and OHT nerves. NaV1.2 expression significantly increased in sham nerves compared with nerves from saline-injected eyes ( $P = 0.0104$ ). Crush significantly reduced NaV1.2 localization compared with naïve and sham nerves ( $P \leq 0.0236$ ). Naïve:  $n = 77$  nodes, saline:  $n = 26$  nodes, sham:  $n = 65$  nodes, OHT: 29 nodes, ONC: 0 nodes. Animal  $n \geq 3$ . **(D, left)** We did not detect a significant difference in node length between conditions ( $P \geq 0.201$ ). **(D, right)** Optic nerve axon paranode length of naïve and saline-injected eyes were similar ( $P > 0.99$ ). Compared with naïve, paranode length significantly decreased in sham, OHT and ONC nerve ( $P \leq 0.0205$ ,  $n \geq 49$ ). OHT significantly reduced paranode extent relative to nerves from saline-injected eyes ( $P = 0.0006$ ,  $n \geq 509$ ). Animal  $n \geq 0.3$ . Statistics: **(C, D)** Kruskal–Wallis one-way ANOVA, Dunn's *post hoc*. Significance indicators: \* $<0.05$ , \*\* $<0.01$ , \*\*\* $<0.001$ , \*\*\*\* $<0.0001$ . Data are presented as mean  $\pm$  SEM.

progression.<sup>24,25–30</sup> Based on this premise, we determined if contralateral excitability is due to changes in nodal NaV1.6 expression flanked by paranodes identified by Caspr1 in longitudinal optic nerve sections (Fig. 2A).<sup>24</sup> We found NaV1.6 accumulation significantly decreased in both sham and crushed nerves compared with nerves from naïve eyes ( $P \leq 0.001$ , Fig. 2C, left). Furthermore, we observed a significant reduction in nodal NaV1.6 intensity in nerves from both saline- and microbead-injected eyes compared with nerves from naïve eyes ( $P \leq 0.008$ ; Fig. 2C, left). We verified

NaV1.6 immunoreactivity by application of a blocking peptide prior to adding the primary antibody. We found NaV1.6 immunofluorescence reduced by the blocking peptide (Supplementary Fig. 2C and D). Based on these results, contralateral hyperexcitability does not appear to be due to increased NaV1.6 expression. Instead, NaV1.6 immunofluorescence decreased in injured and contralateral tissues compared with naïve.

Similar to our results, NaV1.6 immunolabelling is also reduced in optic nerve axons of experimental models of

diseases that cause axon demyelination.<sup>31,32</sup> In both acute and genetic models, demyelination induces the substitution of NaV1.6 for NaV subunit 1.2 (NaV1.2).<sup>31,32</sup> Therefore, we determined if unilateral ocular hypertension or optic nerve crush altered the accumulation of NaV1.2 in optic nerve axon nodes of Ranvier. We did not detect a significant difference in NaV1.2 immunolabelling in optic nerve axons from naïve versus saline ( $P=0.20$ ) or naïve versus sham eyes ( $P=0.58$ ). However, the percent of NaV1.2-positive nodes in the contralateral nerve ( $8.1 \pm 0.86\%$ ) significantly increased compared with nerves from saline-injected eyes ( $+273\%$ ,  $P < 0.0001$ , Fig. 2C, right). We saw NaV1.2 immunostaining within crushed optic nerves (Fig. 2B), but we did not detect NaV1.2 localized within nodes of Ranvier ( $0\%$ , Fig. 2C, right). We confirmed NaV1.2 immunoreactivity by applying a blocking peptide before adding the primary antibody. We found NaV1.2 immunofluorescence diminished by the blocking peptide (Supplementary Fig. 2E and F). Based on these results, expression of NaV1.2 in nodes of Ranvier across naïve and injured tissues appears uncommon and variable, indicating ectopic expression of NaV1.2 is not a likely mechanism driving hyperexcitability in the sham nerve.

As mentioned above, decreased NaV1.6 expression in nodes of Ranvier indicates on-going demyelination.<sup>32,33</sup> We further explored this possibility by measuring node and paranode length. Of course, we observed relatively few intact nodes of Ranvier in crushed nerves (Fig. 2A and B). We did not detect a significant difference in node length in nerves from naïve and experimental animals ( $P=0.16$ ; Fig. 2D, left). However, paranode length was reduced in both sham and crushed nerves compared with nerves from naïve and saline-injected eyes ( $P \leq 0.002$ , Fig. 2D, right). Interestingly, we found 1 week of IOP elevation significantly reduced paranode length compared with nerves from naïve and saline-injected eyes ( $P \leq 0.02$ , Fig. 2D, right). Our results suggest sham surgery, optic nerve crush and ocular hypertension induce demyelination near the nodes of Ranvier as evidenced by increased paranode length.

## Voltage-gated responses of $\alpha$ ON-S RGC drive contralateral optic nerve hyperexcitability

Next, we investigated if contralateral optic nerve hyperexcitability originates from intraretinal mechanisms, and we directly compared pathology caused by IOP elevation versus optic nerve crush on RGCs by measuring physiologic responses to light and current stimulation. We identified two well-characterized alpha-type RGCs,  $\alpha$ ON- and  $\alpha$ OFF-S RGCs, using physiological and morphological signatures.  $\alpha$ ON-S RGCs were determined based on heavy immunolabelling against SMI-32 and dendritic stratification within the inner plexiform layer marked by choline acetyltransferase.  $\alpha$ ON-S RGCs from naïve eyes possessed large somas ( $307.8 \pm 15.2 \mu\text{m}^2$ ) with strong immunoreactivity to

SMI-32 (SMI-32: background intensity =  $6.9 \pm 0.45$ ), and their dendrites ramified within the proximal band of choline acetyltransferase-positive amacrine cell processes, defining the ON sublamina of the inner plexiform layer (Fig. 3A). After 1 week of IOP elevation, we found the morphology of  $\alpha$ ON-S RGCs similar to fellow cells from saline-injected eyes, but  $\alpha$ ON-S RGCs from sham and optic nerve crush eyes showed distinct signs of degeneration (Fig. 3B).

Physiologically,  $\alpha$ ON-S RGCs from naïve and saline eyes maintained similar RMPs ( $-60.9 \pm 0.8$  versus  $-60.4 \pm 0.52$  mV,  $P=0.99$ ; Fig. 3C), and these cells produced a sustained volley of action potentials during light onset (Fig. 3D, left). Similarly, RMP of  $\alpha$ ON-S RGCs from sham eyes ( $-62 \pm 0.92$  mV) was comparable with that of cells from naïve and saline eyes ( $P \leq 0.79$ , Fig. 3C), but the light-evoked peak response of  $\alpha$ ON-S RGCs from sham eyes appeared to exceed that of cells from saline-injected eyes while the sustained component seemed similar (Fig. 3D, left). One week post crush, RMP of  $\alpha$ ON-S RGCs was significantly depolarized ( $-57.1 \pm 1.4$  mV) compared with  $\alpha$ ON-S RGCs in naïve and sham eyes ( $P < 0.05$ , Fig. 3C). Crush degraded both transient and sustained components of the light response of  $\alpha$ ON-S RGCs in the injured eye (Fig. 3D, right). When quantified, we found optic nerve crush significantly blunted the mean spike rate ( $P \leq 0.002$ ), integrated spiking ( $P \leq 0.0006$ ) and light-evoked peak firing rate ( $P \leq 0.004$ ) of  $\alpha$ ON-S RGCs compared with like cells from naïve and sham eyes (Fig. 3E). Intriguingly, we found the light-evoked peak firing rate of  $\alpha$ ON-S RGCs from the sham eye significantly increased compared with cells from saline-injected eyes ( $120.7 \pm 18$  versus  $65.2 \pm 9.2$  spikes/s,  $P < 0.01$ , Fig. 3E, right).

We defined  $\alpha$ OFF-S RGCs by analysing dendritic stratification, SMI-32 immunolabelling and light responses.  $\alpha$ OFF-S RGCs from naïve eyes possessed large somas ( $285.7 \pm 19.97 \mu\text{m}^2$ , Fig. 4A, left) with dendrites arbourizing just beyond the plexus of choline acetyltransferase-positive amacrine cell dendrites, marking the OFF sublamina of the inner plexiform layer (Fig. 4A, right).  $\alpha$ OFF-S RGCs from naïve eyes produced immunoreactivity to SMI-32 ( $6.78 \pm 0.96$ , Fig. 4A, left). The somato-dendritic compartment of  $\alpha$ OFF-S RGCs from saline and sham eyes appeared similar, optic nerve crush appeared to decrease soma size and dendritic arbour complexity (Fig. 4B).

$\alpha$ OFF-S RGCs from naïve ( $-55.75 \pm 0.78$  mV), saline eyes ( $55.2 \pm 0.71$  mV) and sham ( $-53.44 \pm 1.0$  mV) maintained similar RMPs ( $P \geq 0.48$ , Fig. 4C). In response to light onset,  $\alpha$ OFF-S RGCs immediately hyperpolarized, suppressing the initiation of action potentials. Following light offset, these cells typically produced a robust pack of spikes (Fig. 4D).  $\alpha$ OFF-S RGCs from naïve, saline and sham animals produced similar mean ( $P \geq 0.98$ ), integrated response ( $P \geq 0.11$ ) and peak light-induced firing rates ( $P \geq 0.89$ , Fig. 4E). Crush significantly blunted  $\alpha$ OFF-S RGC light-evoked spiking across all measurements relative to cells from naïve and sham animals (mean:  $P \leq 0.0001$ ; integrated:  $P \leq 0.001$ ; peak:  $P \leq 0.007$ ; Fig. 4E). Moreover, optic nerve crush modestly reduced the mean light-evoked spike rate of  $\alpha$ OFF-S RGCs

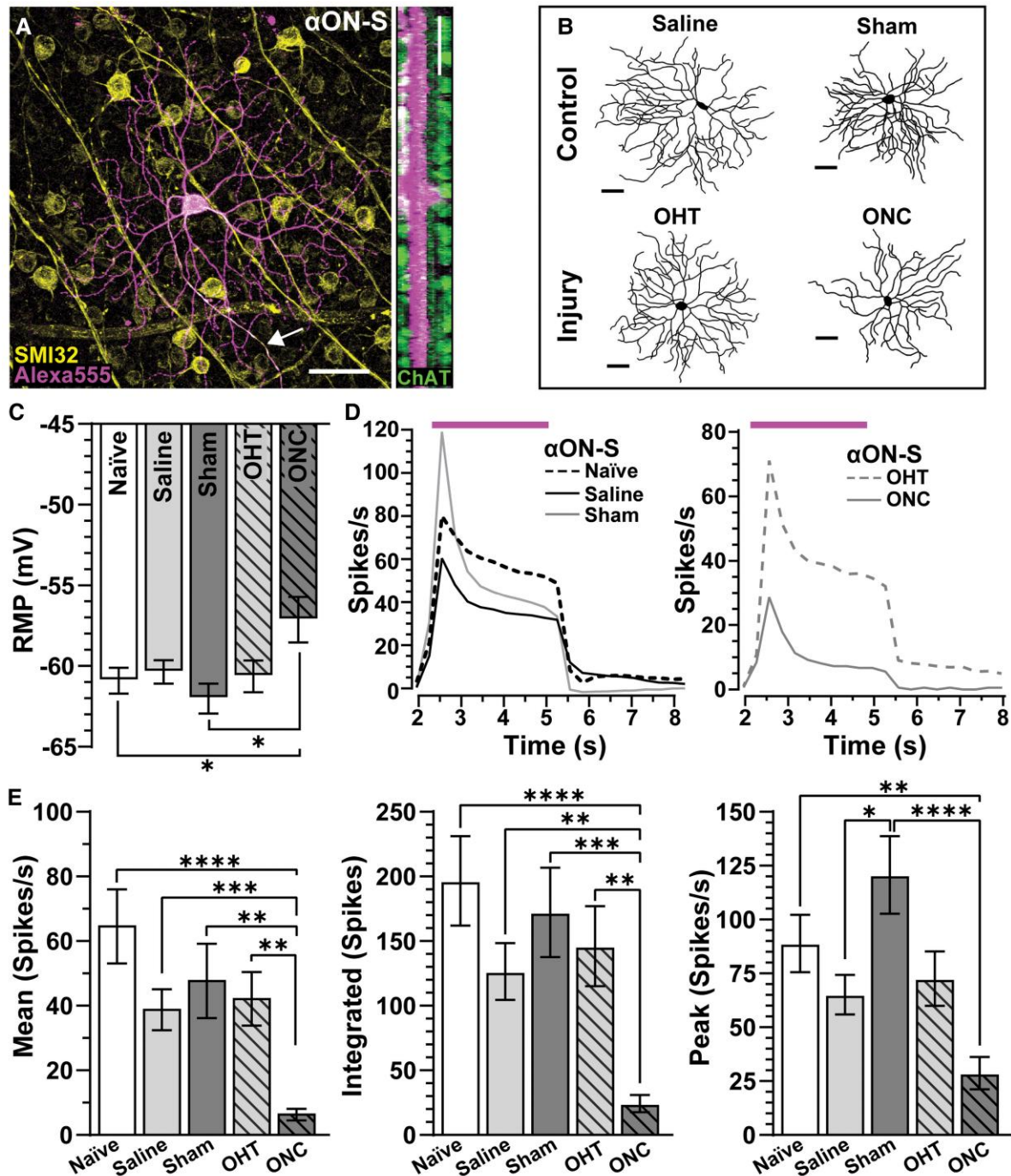


**Figure 3** Optic nerve crush depolarizes RMP and decreases light-evoked responses of  $\alpha$ ON-S RGCs. **(A)** Confocal micrograph of Alexa 555 filled naive  $\alpha$ ON-S RGC. Retinas were immunolabelled for SMI-32. Orthogonal rotation shows  $\alpha$ ON-S RGC dendrites ramify in the ON sublamina of the inner plexiform layer defined by choline acetyltransferase (ChAT). Arrow indicates RGC axon. Scale bars = 50  $\mu$ m. **(B)** Reconstructed and skeletonized  $\alpha$ ON-S RGCs from saline, OHT, sham and ONC retinas. Scale bars = 50  $\mu$ m. **(C)** ONC depolarized  $\alpha$ ON-S RGCs RMP compared with like cells from naive ( $P=0.05$ ,  $n \geq 16$ ) and sham retinas ( $P=0.03$ ,  $n \geq 11$ ). **(D, left)** Averaged histograms (3 ms bins) of light-evoked response of naive, saline and sham  $\alpha$ ON-S RGCs. **(D, right)** ONC reduced light responses of  $\alpha$ ON-S RGCs compared with OHT (right). **(E)** Compared with like cells from naive retinas, light responses (mean, integrated and peak) of  $\alpha$ ON-S RGCs from sham and saline retinas were similar ( $P > 0.99$ ,  $n \geq 12$ ). ONC significantly reduced light-induced responses (mean, integrated, peak) of  $\alpha$ ON-S RGCs compared with naive ( $P < 0.0001$ ,  $n \geq 17$ ). Peak light response is significantly greater in sham  $\alpha$ ON-S RGCs compared with saline  $\alpha$ ON-S RGCs ( $P=0.02$ ,  $n \geq 12$ ). After 1Wk, there is no difference in mean, integrated, or peak light responses for OHT  $\alpha$ ON-S RGCs compared with saline  $\alpha$ ON-S RGCs ( $P > 0.99$ ,  $n \geq 16$ ). Statistics: **(C)** One-way ANOVA and Tukey's *post hoc*. **(E)** Kruskal–Wallis one-way ANOVA, Dunn's *post hoc*. Significance indicators: \* $<0.05$ , \*\* $<0.01$ , \*\*\* $<0.001$ , \*\*\*\* $<0.0001$ . Data presented as mean  $\pm$  SEM.

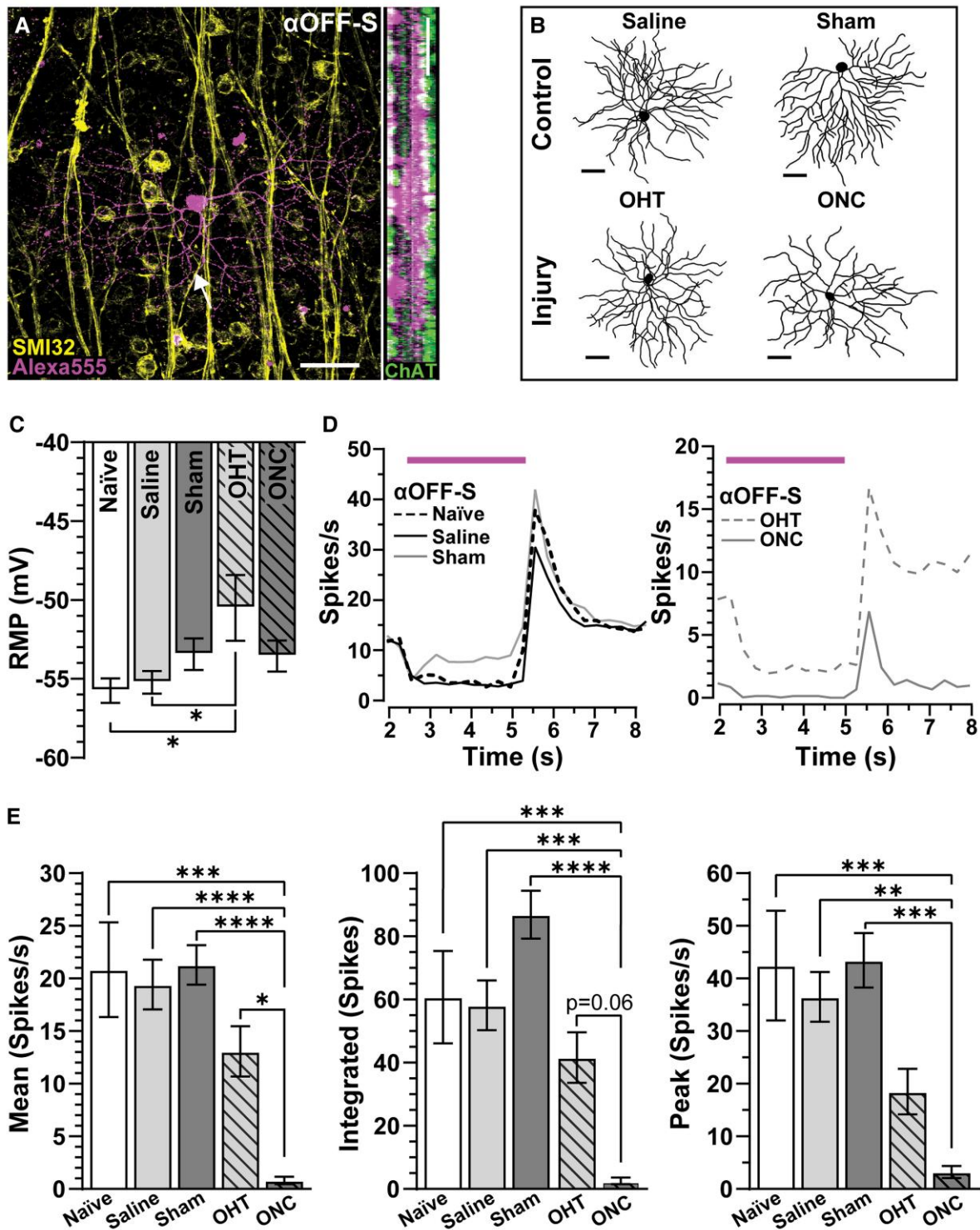


**Figure 4** Optic nerve crush diminishes light-evoked responses of  $\alpha$ OFF-S RGCs. (A) Confocal image of Alexa 555 filled  $\alpha$ OFF-S RGC in a naive retina immunolabelled against SMI-32. Orthogonal rotation shows  $\alpha$ ON-S RGC dendrites project in and beyond the OFF sublamina of the inner plexiform layer as defined by ChAT. Arrow shows the RGC axon. Scale bars = 50  $\mu$ m. (B) Example  $\alpha$ OFF-S RGCs, reconstructed and skeletonized, from saline, OHT, sham and ONC retinas. Scale bars = 50  $\mu$ m. (C) OHT significantly depolarized  $\alpha$ OFF-S RGCs RMP compared with like cells of naive and saline retinas ( $P \leq 0.023$ ,  $n \geq 8$ ). (D, left) Averaged histogram of spontaneous and light-evoked spiking of  $\alpha$ OFF-S RGCs from naive, saline and sham retinas. (D, right) ONC reduced light responses of  $\alpha$ OFF-S RGCs compared with OHT. (E) Light responses (mean, integrated and peak) of  $\alpha$ OFF-S RGCs from naive, saline and sham eyes were similar ( $P \geq 0.98$ ,  $n \geq 12$ ). ONC significantly blunted mean ( $P \leq 0.0001$ ), integrated ( $P \leq 0.001$ ) and peak ( $P \leq 0.0003$ ) light-driven responses for ONC  $\alpha$ OFF-S RGCs compared with naive and sham  $\alpha$ OFF-S RGCs ( $n \geq 10$ ). Statistics: (C, E) One-way ANOVA and Tukey's *post hoc*. Significance indicators: \* $<0.05$ , \*\* $<0.01$ , \*\*\* $<0.001$ , \*\*\*\* $<0.0001$ . Data are presented as mean  $\pm$  SEM.

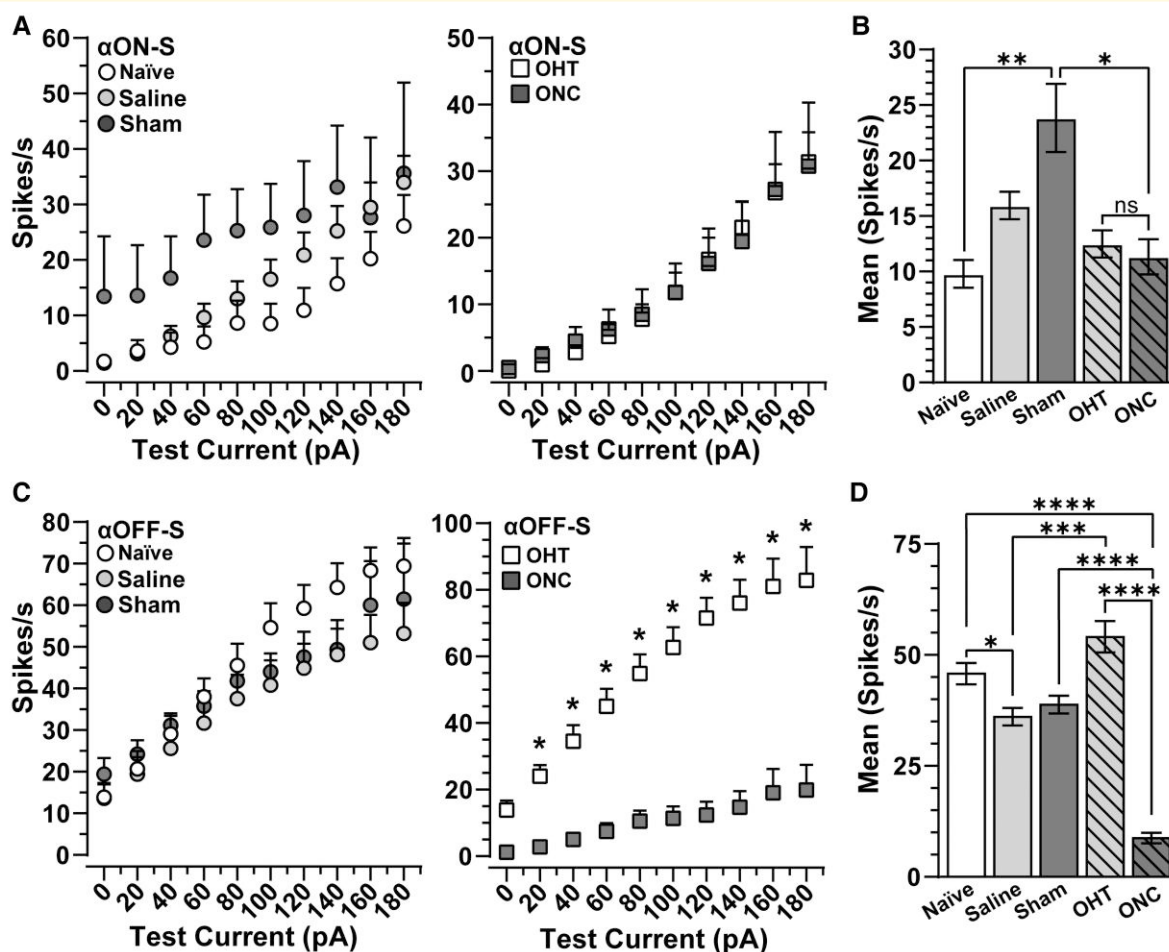


**Figure 5** Optic crush enhances current-evoked spiking in  $\alpha$ ON-S RGCs of the sham nerve. (A, left)  $\alpha$ ON-S RGCs of sham nerves produce higher spike rates than like cells from naïve and saline eyes to depolarizing currents up to 140 pA ( $n \geq 7$ ). (A, right) Current-evoked spike rates of  $\alpha$ ON-S RGCs from ONC eyes are similar to  $\alpha$ ON-S RGCs from OHT eyes (right) ( $n \geq 13$ ). (B)  $\alpha$ ON-S RGCs from naïve and saline eyes produce similar mean current-evoked spike rates ( $P = 0.12$ ). Mean current-evoked spike rate is significantly greater in sham  $\alpha$ ON-S RGCs compared with naïve  $\alpha$ ON-S RGCs ( $P = 0.002$ ). (C, left)  $\alpha$ OFF-S RGCs from naïve, saline and sham eyes produce similar spike rates in response to depolarizing currents up to 180 pA ( $n \geq 12$ ). (C, right) ONC reduced responses to depolarizing current in  $\alpha$ OFF-S RGCs versus OHT  $\alpha$ OFF-S RGCs ( $P \leq 0.01$ ,  $n \geq 6$ ). (D) Mean current-evoked spike rate is decreased for saline  $\alpha$ OFF-S RGCs compared with naïve  $\alpha$ OFF-S RGCs ( $P < 0.01$ ). OHT increases  $\alpha$ OFF-S RGC spike rate compared with saline  $\alpha$ OFF-S RGCs ( $P < 0.0001$ ). Conversely, ONC  $\alpha$ OFF-S RGCs have a significantly lower mean current-evoked spike rate compared with sham  $\alpha$ OFF-S RGCs ( $P < 0.0001$ ). Statistics: (A, C) Two-way repeated measures ANOVA with Bonferroni's *post hoc*. (B) Kruskal–Wallis one-way ANOVA, Dunn's *post hoc*. (D) One-way ANOVA and Tukey's *post hoc*. Significance indicators: \* $<0.05$ , \*\* $<0.01$ , \*\*\* $<0.001$ , \*\*\*\* $<0.0001$ . Data presented as mean  $\pm$  SEM.

when compared with cells from microbead-injected eyes ( $P = 0.05$ , Fig. 4E).

Next, we determine how intrinsic mechanisms of  $\alpha$ ON- and  $\alpha$ OFF-S RGCs contribute to enhanced excitability of the optic nerve of sham eyes and degradation of compound action potentials of nerved subjected to crush by measuring spike output to depolarizing current injections in the absence of light. We found  $\alpha$ ON-S RGCs from naïve and saline eyes produced negligible spontaneous activity (0 pA test current:  $1.6 \pm 0.86$  versus  $1.43 \pm 0.64$  spikes/s, respectively) compared with cells from the sham eye ( $13.43 \pm 10.85$  spikes/s,  $P \leq 0.05$ , Fig. 5A, left). Current-evoked responses of  $\alpha$ ON-S RGCs from sham eyes remained elevated versus

naïve and saline, at smaller test currents (Fig. 5A, left). To the counter, responses to depolarizing current injections of  $\alpha$ ON-S RGCs from microbead-injected eyes and optic nerve crush eyes appeared strikingly similar (Fig. 5A, right). When averaged across current steps, we found spiking significantly increased in  $\alpha$ ON-S RGCs from sham eyes versus cells from naïve eyes by 143% ( $23.8 \pm 3.1$  versus  $9.8 \pm 1.2$  spikes/s,  $P = 0.0015$ , Fig. 5B). However, unlike light-evoked responses (Fig. 3D and E), we did not detect a significant difference in average responses of  $\alpha$ ON-S RGCs from microbead-injected eyes and optic nerve crush eyes to current stimulation ( $P > 0.99$ , Fig. 5B). These results suggest mechanisms independent of those generating light responses of  $\alpha$ ON-S

RGCs remain intact while pre- and post-synaptic mechanisms mediating light-evoked responses appear to falter 1 week after traumatic optic neuropathy. Moreover, enhanced excitability of  $\alpha$ ON-S RGCs from sham eyes mirrors hyperexcitability in the optic nerve compound action potential from sham animals.

Above, we observed injecting saline slightly increased average current-evoked spiking in  $\alpha$ ON-S cells, and sham surgery significantly enhanced excitability (Fig. 5A and B). For OFF-S RGCs, saline injection significantly depressed excitability compared with naïve cells ( $P = 0.006$ , Fig. 5C and D). Though also reduced, current-evoked responses of OFF-S RGCs from sham eyes were statistically comparable with cells from naïve eyes ( $P = 0.20$ , Fig. 5C and D). Interestingly, in corroboration with our previous findings,<sup>23–25</sup> we found IOP elevation increased  $\alpha$ OFF-S RGC excitability compared with like cells from saline-injected eyes ( $P < 0.001$ , Fig. 5C and D). On the other hand, responses of  $\alpha$ OFF-S RGCs from saline-injected eyes decreased compared with naïve. Finally, optic nerve crush significantly reduced current-evoked responses of  $\alpha$ OFF-S RGCs compared with naïve, sham and microbead-injected eyes ( $P \leq 0.0001$ , Fig. 5C, right, D). In the context of our previous work,<sup>19,23–25</sup> these results suggest intrinsic voltage-gated responses of  $\alpha$ ON-S RGCs drive contralateral optic nerve axon hyperexcitability following crush (Fig. 5A and B), and 1 week of ocular hypertension piques intrinsic mechanisms of  $\alpha$ OFF-S RGCs, increasing excitability compared with like cells from saline-injected eyes (Fig. 5C and D). However, this increased excitability is relative to cells of the saline eye because either saline injection or stress induced by ocular hypertension reduced  $\alpha$ OFF-S RGC excitability compared with naïve.

## Dendritic pruning is accelerated by optic nerve crush compared with ocular hypertension

We noted SMI-32 immunolabelling increased in  $\alpha$ ON-S RGCs from sham eyes, while SMI-32 immunostaining in  $\alpha$ ON-S RGCs from other conditions appeared similar to like cells from naïve eyes (Fig. 6A). As expected, neither saline injection, ocular hypertension, nor crush produced an appreciable change in  $\alpha$ ON-S RGC SMI-32 labelling compared with like cells from naïve eyes ( $P \geq 0.96$ , Fig. 6B). However, at 1 week post crush, SMI-32 significantly accumulated in  $\alpha$ ON-S RGC somas from sham eyes ( $12.6 \pm 1.67$ ) compared with cells from naïve ( $6.9 \pm 0.45$ ) and saline eyes ( $6.5 \pm 0.43$ ,  $P \leq 0.036$ , Fig. 6B). In line with this result, the cross-sectional area of  $\alpha$ ON-S RGC somas from sham eyes ( $429.5 \pm 35.3 \mu\text{m}^2$ ) significantly increased 36–39% compared with  $\alpha$ ON-S RGCs from naïve ( $307.8 \pm 15.2 \mu\text{m}^2$ ) and saline-injected eyes ( $309.7 \pm 10.2 \mu\text{m}^2$ ,  $P \leq 0.017$ ) and fellow cells from eyes receiving optic nerve crush ( $307.1 \pm 22.1 \mu\text{m}^2$ ,  $P = 0.019$ , Fig. 6C). Despite changes in somatic SMI-32 labelling and area, dendritic complexity of  $\alpha$ ON-S RGCs from sham eyes remained intact compared with cells from sham and saline-injected eyes as determined by the

number of dendritic intersections ( $P \geq 0.13$ , Fig. 6D, left), branch points ( $P > 0.91$ ), total dendritic length ( $P = 0.76$ ) and dendritic field area ( $P = 0.82$ , Fig. 6E). Optic nerve crush reduced the number of dendritic intersections ( $P \leq 0.03$ , Fig. 6D, right) and branch points ( $-28\%$ ,  $37.4 \pm 2.2$  versus  $52.4 \pm 3.9$  branch points,  $P = 0.029$ ) of  $\alpha$ ON-S RGCs in the directly affected eye compared with cells from microbead-injected eyes (Fig. 6E). As anticipated,<sup>34</sup> these results suggest crush accelerates dendritic degeneration in  $\alpha$ ON-S RGCs compared with ocular hypertension. Additionally, our findings suggest unilateral lesion produces signatures of degeneration in  $\alpha$ ON-S RGCs of the contralateral, sham and eye.

In contrast to  $\alpha$ ON-S RGCs, sham surgery did not appear to produce a significant change in SMI-32 expression in  $\alpha$ OFF-S RGCs. However, optic nerve crush seemed to reduce SMI-32 expression in this cell type (Fig. 7A). Quantification of SMI-32 immunolabelling confirmed our observations: SMI-32 labelling in  $\alpha$ OFF-S RGCs from sham eyes was comparable with that of  $\alpha$ OFF-S RGCs from naïve and saline-injected eyes ( $P \geq 0.147$ ), and optic nerve crush significantly reduced SMI-32 labelling by 49% in  $\alpha$ OFF-S RGCs versus like cells from sham eyes ( $3.37 \pm 0.35$  versus  $6.65 \pm 1.31$ ,  $P = 0.047$ , Fig. 7B). Along with a reduction in SMI-32 expression, optic nerve crush significantly reduced soma area of  $\alpha$ OFF-S RGCs by 28% compared with cells from sham eyes ( $218 \pm 9.9$  versus  $305 \pm 17.7 \mu\text{m}^2$ ,  $P = 0.01$ , Fig. 7C). Cross-sectional soma area of  $\alpha$ OFF-S RGCs from saline and sham eyes was similar to  $\alpha$ OFF-S RGCs from naïve eyes ( $P > 0.99$ ).

Regarding dendritic arbour morphology, Sholl analysis indicated similar number of dendritic intersections in  $\alpha$ OFF-S RGCs from naïve, saline and sham eyes ( $P \geq 0.15$ , Fig. 7D, left). Interestingly, in contrast to  $\alpha$ ON-S RGCs (Fig. 6D, right), we found crush did not produce a significant change in the number of dendritic intersections when compared with like cells from microbead-injected eyes ( $P \geq 0.93$ , Fig. 7D, right). However, compared with  $\alpha$ OFF-S RGCs from naïve and sham eyes, optic nerve crushed significantly diminished the number of dendritic branching points ( $P \leq 0.05$ , Fig. 7E). Similar to our results from Sholl analysis, neither optic nerve crush nor sham surgery significantly affected dendritic length ( $P > 0.99$ ) or field area ( $P > 0.99$ ) of  $\alpha$ OFF-S RGCs compared with fellow cells from naïve eyes (Fig. 7E).

## Discussion

### Unilateral optic nerve trauma increased excitability of contralateral fibres through enhanced excitability of $\alpha$ ON-S RGCs

Our main physiologic result is unilateral optic nerve trauma significantly enhanced excitability of fibres comprising the contralateral nerve in the absence of pathologic indications (Fig. 1B–F). In the context of previous findings from our

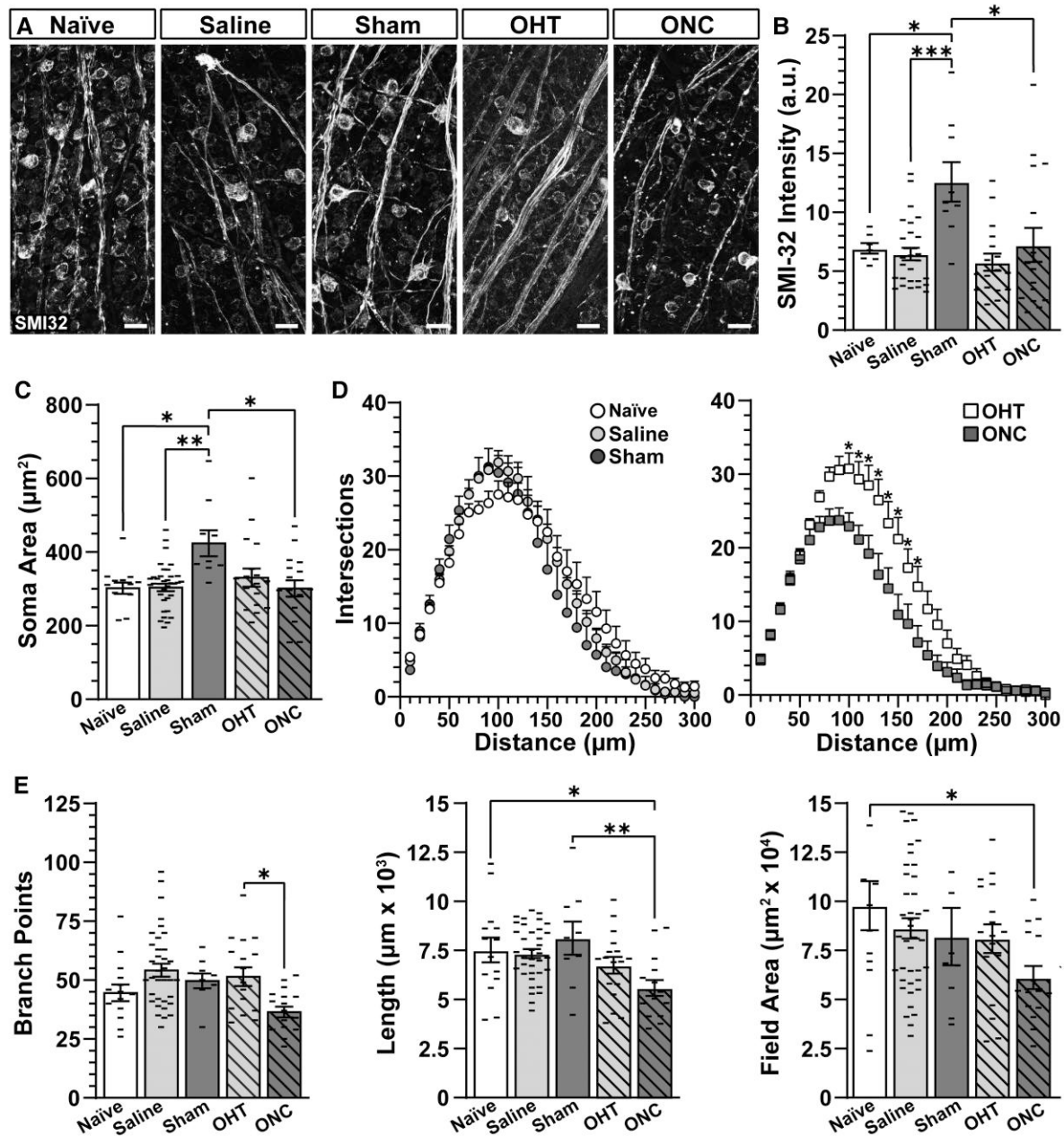


**Figure 6 Unilateral optic nerve crush produces bilateral pro-degenerative responses in  $\alpha$ ON-S RGCs.** (A) Representative confocal micrographs of SMI-32 immunolabelled whole-mount retinas. Scale bars = 25  $\mu$ m. (B) Somatic SMI-32 intensity increased in sham  $\alpha$ ON-S RGCs compared with like cells from naïve ( $P = 0.04$ ,  $n \geq 7$ ) and saline retinas ( $P < 0.001$ ,  $n \geq 9$ ). ONC significantly reduced SMI-32 expression in  $\alpha$ ON-S RGCs compared with sham  $\alpha$ ON-S RGCs ( $P = 0.01$ ,  $n \geq 9$ ). (C) Soma areas are larger in sham  $\alpha$ ON-S RGCs compared with naïve ( $P \leq 0.02$ ) and saline  $\alpha$ ON-S RGCs ( $P = 0.006$ ,  $n \geq 9$ ). ONC decreased  $\alpha$ ON-S RGC soma area relative to sham ( $P = 0.02$ ,  $n \geq 9$ ). (D, left) Sholl analysis indicates similarity in dendritic complexity of  $\alpha$ ON-S RGCs from naïve, saline and sham eyes ( $P = 0.16$ ,  $n \geq 9$ ). (D, right) ONC significantly reduced dendritic intersections of  $\alpha$ ON-S RGCs compared with like cells from OHT eyes ( $P < 0.05$ ). (E)  $\alpha$ ON-S RGCs from naïve, saline and sham retinas possess similar dendritic arbour morphologies based on branch points, dendritic length and field area ( $P \geq 0.22$ ,  $n \geq 9$ ). Total dendritic length is significantly reduced in  $\alpha$ ON-S RGCs following ONC compared with naïve ( $P < 0.05$ ) and sham  $\alpha$ ON-S RGCs ( $P = 0.01$ ,  $n \geq 9$ ). Dendritic field area is reduced by ONC in  $\alpha$ ON-S RGCs compared with naïve  $\alpha$ ON-S RGCs ( $P < 0.05$ ,  $n \geq 9$ ). Statistics: (B, C and E) One-way ANOVA and Tukey's *post hoc*. (D) Two-way repeated measures ANOVA with Bonferroni's *post hoc* test. Significance indicators: \* $< 0.05$ , \*\* $< 0.01$ , \*\*\* $< 0.001$ , \*\*\*\* $< 0.0001$ . Data are presented as mean  $\pm$  SEM.

laboratory and others, we suggest hyperexcitability is an early indicator of neurodegeneration, occurring prior to out-right axon degeneration.<sup>23,24,25–35,36</sup> This claim is further

evidenced by neurodegenerative signatures, including reduced nodal NaV1.6 expression (Fig. 2A and C), reduced paranode length (Fig. 2D), enhanced accumulation of

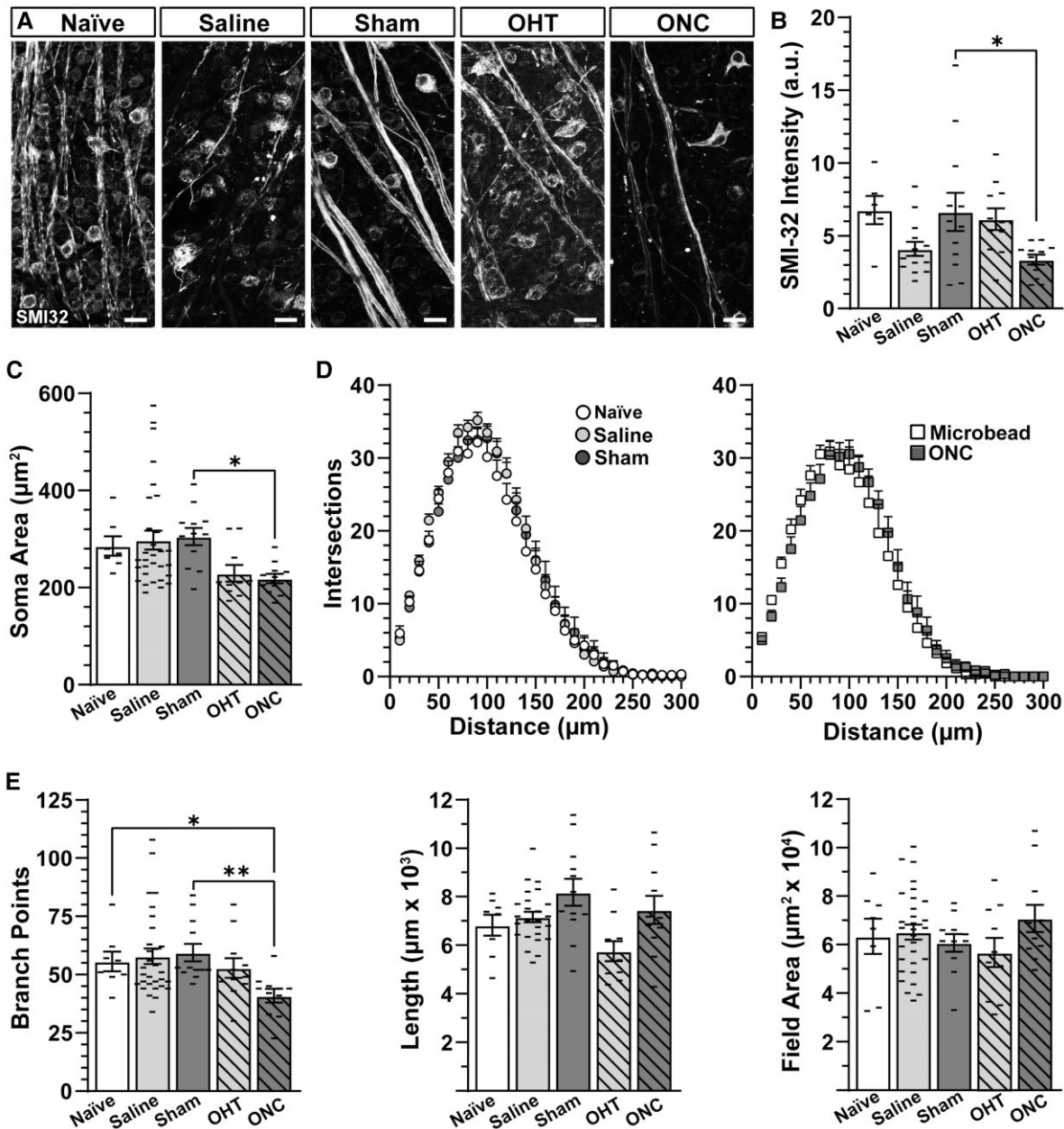


**Figure 7** Optic nerve crush piques mechanisms controlling dendritic branch points in  $\alpha$ OFF-S RGCs. **(A)** Example confocal images of SMI-32 immunolabelled whole-mount retinas. Scale bars = 25  $\mu$ m. **(B)** ONC reduced SMI-32 accumulation in  $\alpha$ OFF-S RGCs relative to sham  $\alpha$ OFF-S RGCs ( $P < 0.05$ ,  $n \geq 11$ ). **(C)** ONC decreased  $\alpha$ OFF-S RGC soma area compared with like cells from sham eyes ( $P = 0.01$ ,  $n \geq 11$ ). **(D, left)** Sholl analysis indicated the number of dendritic intersection is similar for  $\alpha$ OFF-S RGCs from naïve, saline and sham eyes ( $P = 0.96$ ,  $n \geq 6$ ). **(D, right)** The number of dendritic intersections is also similar for  $\alpha$ OFF-S RGCs from ONC and OHT eyes ( $P = 0.48$ ,  $n \geq 10$ ). **(E)** There is no difference in the number of branch points, dendritic length or dendritic field area of saline and sham  $\alpha$ OFF-S RGCs compared with naïve ( $P \geq 0.99$ ,  $n \geq 8$ ). ONC significantly reduced the number of branch points in  $\alpha$ OFF-S RGCs compared with like cells from naïve ( $P = 0.05$ ,  $n \geq 8$ ) and sham retinas ( $P = 0.003$ ,  $n \geq 11$ ). Statistics: **(B)** One-way ANOVA and Tukey's *post hoc*. **(C and E)** Kruskal–Wallis one-way ANOVA, Dunn's *post hoc*. **(D)** Two-way repeated measures ANOVA with Bonferroni's *post hoc* test. Significance indicators: \* $<0.05$ , \*\* $<0.01$ , \*\*\* $<0.001$ , \*\*\*\* $<0.0001$ . Data are presented as mean  $\pm$  SEM.

SMI-32 (Fig. 6A and B) and enlarged soma area of  $\alpha$ ON-S RGCs that send projections to the contralateral nerve (Fig. 6C).<sup>31,32–37,38,39</sup> Based on these data, we propose unilateral trauma produces subtle indicators of degeneration in  $\alpha$ ON-S RGCs and their axons of the contralateral eye.

Enhanced excitability of the contralateral nerve is not due to alterations of nodal NaV1.6. In fact, NaV1.6 expression in contralateral nerve axons significantly decreased compared with nerves from naïve and saline-injected eyes (Fig. 2A and C). We found paranode length decreased in

axons of the contralateral nerve versus nerves of naïve and saline-injected eyes (Fig. 2D). Collectively, these axonal stress responses indicate demyelination in the contralateral nerve, and all else being equal, would result in reduced compound action potentials.<sup>31,32–39,40,41,42</sup>

Our data indicates intraretinal mechanisms drive enhanced excitability in the contralateral nerve.  $\alpha$ ON-S RGCs from sham eyes produced greater firing rate to depolarizing current injections compared with responses of like cells from saline-injected and naïve eyes, respectively (Fig. 5B), exhibited increased accumulation of SMI-32 (Fig. 6A and B) and increased soma area (Fig. 6C). Enhanced excitability of  $\alpha$ ON-S RGCs within the sham eye appears to originate from intrinsic voltage-gated mechanisms. We found mean light-evoked responses and dendritic profiles of  $\alpha$ ON-S RGCs from sham eyes unchanged (Figs 3 and 6). However, in the absence of light, current-driven responses of these very cells increased. These findings suggest mechanisms of  $\alpha$ ON-S RGCs that contribute to spike initiation may be piqued by sham surgery or stress transduced from the contralateral, crushed and nerve.

While responses of  $\alpha$ ON-S RGCs from the sham eye increased, light- and current-evoked responses of  $\alpha$ OFF-S RGC from the same eye remained intact (Figs 4D, E and 5C, D). Furthermore,  $\alpha$ OFF-S RGCs projecting to the contralateral nerve exhibited similar SMI-32 accumulation, soma area and dendritic arbour profiles compared with like cells from naïve and saline-injected eyes (Fig. 7). Based on these data, the summed responses of  $\alpha$ ON- and  $\alpha$ OFF-S RGC projections within the contralateral nerve would tilt towards hyperexcitability, which might be a compensatory response to loss of connections between RGC axons and central targets of the injured projection.<sup>6</sup> This hyperexcitability in contralateral  $\alpha$ ON-SRGC may be due to increased NaV channels within unmyelinated axon segments, similar to our findings during early glaucoma.<sup>25</sup>

Several studies indicate immune cell activation in the contralateral nerve following unilateral injury.<sup>7,8,9,10,11,12</sup> Hyperexcitability may be supported by reactive microglia that secrete pro-inflammatory cytokines such as tumour necrosis factor alpha (TNF- $\alpha$ ).<sup>43</sup> Interestingly, TNF- $\alpha$  increases NaV1.1, 1.2 and 1.6 channel mRNA expression and enhances NaV currents in cortical neurons.<sup>44</sup> In the light of these data and our results, pro-inflammatory signals may prompt upregulation of NaV channels along unmyelinated axon segments of remaining RGCs that project through the contralateral nerve, inducing hyperexcitability.

Intriguingly, we also noticed 1 week of IOP elevation influences contralateral, saline-injected, tissues. We found immunolabelling for NaV1.6 within nodes of Ranvier significantly diminished, and current-evoked responses of  $\alpha$ OFF-S RGCs reduced by  $\sim$ 22% compared with naïve (Figs 2C and 5D). In contrast, IOP elevation tended to increase excitability of  $\alpha$ ON-S RGCs in saline-injected eye (+50%), although this result was not statistically significant relative to like cells from naïve eyes (Fig. 5B). Interestingly,

both  $\alpha$ ON-S and  $\alpha$ OFF-S RGCs have greatest density in the temporal-dorsal retina in mouse.<sup>45</sup> Based on our physiologic results and topography of these RGC types, it might be the case that retrograde signals from central mechanisms differentially influence excitability in  $\alpha$ ON- and  $\alpha$ OFF-S RGCs during unilateral injury as a form of compensation, and this compensation is exemplified in distinct RGCs with overlapping receptive fields that occupy similar topographical space.

## Pathologic progression of optic nerve trauma versus IOP elevation

Glaucomatous and traumatic optic neuropathy differ in both aetiology and rate of progression. However, evidence suggest common pathologic mechanisms that distinctly affect RGC bodies and axons.<sup>19–46,47,48</sup> About 40 h post-optic nerve crush, axons distal to the injury-site fragment, while axons near the nerve head remain intact.<sup>47</sup> A few hours later, axons proximal to the nerve head also fragment.<sup>47</sup> At this time, the density of RGC bodies and axons is reduced by about 30%.<sup>49</sup> Degeneration continues over time, and after 1 week, about 60% of RGC bodies and axons are lost (Fig. 1B and D, Supplementary Fig. 1).<sup>49</sup>

Previously, we have demonstrated progression of axonopathy and RGC degeneration during glaucoma, using the microbead occlusion model, by tracking deficits in anterograde axon transport of CTB to the SC, analysis of optic nerve axon density and RGC density. We found graduated deficits in RGC axon transport to the SC, optic nerve axon density and RGC bodies following 2–8 weeks of IOP elevation. Anterograde axon transport of CTB to the SC sharply declines by 40–50% after 2–4 weeks of IOP elevation, respectively.<sup>25</sup> However, this duration of IOP elevation does not cause significant loss of RGC bodies or optic nerve axons.<sup>19–21</sup> Following 5 weeks of ocular hypertension, anterograde axon transport of CTB remained reduced by half, but axon density significantly decreased by  $\sim$ 20% while the retina maintained a full complement of RGC bodies.<sup>20</sup> After 7–8 weeks of IOP elevation, transport of CTB to the SC is negligible and RGC body and axon density is reduced by about 50% (Fig. 1B and D).<sup>15,49,50</sup> Collectively, these results indicate degeneration caused by optic nerve crush after 1 week is roughly equivalent to 2 months of IOP elevation.

One day after optic nerve crush, the density of nodes of Ranvier localized to axons distal and anterior to the injury site is reduced.<sup>51</sup> After 7 days, nodes of Ranvier and constituent NaV1.6 are largely absent (Fig. 2).<sup>51</sup> As a corollary, 5–7 days post crush, the optic nerve compound action potential is reduced by 65–95%, respectively (Fig. 1E and F).<sup>52,53</sup> The visual evoked potential is reduced by  $\sim$ 75% 1 week post crush.<sup>54</sup>

As expected, the influence of IOP elevation on axonal microarchitecture appears to be more subtle compared with crush. One week of IOP elevation modestly reduced paranode length and NaV1.6 immunolabelling (Fig. 2), and this level of reduction in nodal NaV1.6 localization appears to

generalize 5 weeks post-microbead injection.<sup>55</sup> However, following 1–2 weeks of IOP elevation by microbead occlusion, we found the optic nerve compound action potential remained intact (Fig. 1E and F).<sup>24</sup> The influence of ocular hypertension by microbead occlusion on the optic nerve compound potential is unknown for later time points, but we have previously noted a modest reduction in the N1 component of the visual evoked potential after 4 weeks.<sup>56</sup> After 2 months of IOP elevation, the visual evoked potential is significantly diminished by ~45%.<sup>57</sup> Overall, these results suggest the impact of optic nerve crush after 1 week on cortical vision is more pronounced compared with 2 months of IOP elevation.

Previous results indicate optic nerve crush reduces ganglion cell/nerve fibre layer thickness and the photopic negative response, which is largely generated by RGCs.<sup>58,59</sup> Here, we refined this investigation by examining the influence of optic nerve crush and IOP elevation on the morphology and physiology of two well-characterized RGCs—the  $\alpha$ ON-S and  $\alpha$ OFF-S RGCs.<sup>19–60,61,62</sup> Following 1 week, optic nerve crush significantly depolarized RMP and impaired light-evoked voltage-gated responses of both  $\alpha$ ON-S and  $\alpha$ OFF-S RGCs (Figs 3C–E, and 4C–E). Interestingly, we found depolarizing current-evoked responses of  $\alpha$ ON-S RGCs projecting to the crushed nerve comparable with responses of fellow cells from naïve eyes (Fig. 5A and B). This finding contrasts with the influence of optic nerve crush on current-evoked responses of  $\alpha$ OFF-S RGCs where optic nerve crush significantly reduced spiking in these cells (Fig. 5C and D). Our data support the notion that  $\alpha$ ON-S RGC, also known as the M4 intrinsically photosensitive RGCs, axons are less vulnerable to injury.<sup>63,64,65,66</sup> Additionally, our results support the idea that OFF RGCs are more susceptible to injury compared with ON RGCs.<sup>23–60,61–67,68,69</sup>

One week of IOP elevation did not significantly affect light- or current-evoked responses of  $\alpha$ ON-S or  $\alpha$ OFF-S RGCs when compared with like cells from naïve eyes (Figs 3–5), although RMP of  $\alpha$ OFF-S RGCs was significantly more depolarized by ocular hypertension (Fig. 4C), a result similar to our previous findings.<sup>23–25</sup> In earlier reports, we found 2 weeks of IOP elevation significantly depolarized RMP and increased light- and current-evoked responses of  $\alpha$ ON-S or  $\alpha$ OFF-S RGC.<sup>23–25</sup> This IOP-induced enhanced excitability appears to be due, in part, to increased accumulation of NaV1.6 channels along intraretinal ganglion cell unmyelinated axons.<sup>25</sup> After 4 weeks of ocular hypertension, light-evoked excitability of both  $\alpha$ ON-S and  $\alpha$ OFF-S RGCs decreased along with NaV1.6 and NaV1.2 immunolabelling within unmyelinated RGC axon segments.<sup>22–25</sup> While the current-evoked excitability of  $\alpha$ OFF-S RGCs decreased after 4 weeks of IOP elevation, responses of  $\alpha$ ON-S RGCs to depolarizing currents remained intact.<sup>19</sup> Based on these results, mechanisms driving the light response of both ON and OFF RGCs appear to be most sensitive to optic nerve injury,<sup>34,60,61</sup> and responses produced by unmyelinated axons of  $\alpha$ ON-S RGCs are less responsive to injury.

Morphologically, optic nerve crush significantly reduced  $\alpha$ ON-S and  $\alpha$ OFF-S RGC dendritic branching (Figs 6D and

7D). In corroboration, others have also found RGC dendritic arbour complexity and post-synaptic density 95 labelling are significantly diminished 7 days post-optic nerve crush.<sup>34</sup> Following 1 week of IOP elevation, we did not detect a significant change in dendritic arbour morphology in  $\alpha$ ON-S and  $\alpha$ OFF-S RGCs (Figs 6 and 7). Two to 4 weeks of IOP elevation significantly reduced  $\alpha$ ON-S and  $\alpha$ OFF-S RGC dendritic complexity.<sup>19–25</sup> Therefore, dendritic arbour pruning appears to be an early response to optic nerve stress for both RGC types.

## Conclusion

These studies indicate unilateral optic neuropathy produces bilateral effects on intra- and extraretinal mechanisms controlling RGC dendritic excitation and axon excitability. Our results support the prevailing notion that solely using internal saline injection or sham surgery as controls is inadvisable. Moreover, our findings suggest susceptibility to injury is dependent on RGC type. Follow-up studies should determine the influence of anterograde versus retrograde signals on compensatory mechanisms evoked during degeneration.

## Acknowledgement

The authors thank Dr Purnima Ghose for performing optic nerve sectioning and Brian Carlson for general laboratory assistance.

## Funding

Support provided by a departmental unrestricted award by the Research to Prevent Blindness Inc. (D.J.C.), Bright Focus Foundation (G2022011S, M.L.R.), and National Institutes of Health (NIH) grants EY017427 (D.J.C.), EY024997 (D.J.C.) and EY008126 (D.J.C.). Imaging supported through the Vanderbilt University Medical Center Cell Imaging Shared Resource core facility and NIH grants CA68485, DK20593, DK58404 and DK59637.

## Competing interests

The authors report no competing interests.

## Supplementary material

Supplementary material is available at *Brain Communications* online.

## References

1. Dohmen C, Sakowitz OW, Fabricius M, *et al.* Spreading depolarizations occur in human ischemic stroke with high incidence. *Ann Neurol.* 2008;63:720–728.

2. Somjen GG. Mechanisms of spreading depression and hypoxic spreading depression-like depolarization. *Physiol Rev.* 2001;81:1065-1096.
3. Quigley HA, Addicks EM. Regional differences in the structure of the lamina cribrosa and their relation to glaucomatous optic nerve damage. *Arch Ophthalmol.* 1981;99:137-143.
4. Quigley HA. Glaucoma. *Lancet.* 2011;377:1367-1377.
5. Broman AT, Quigley HA, West SK, et al. Estimating the rate of progressive visual field damage in those with open-angle glaucoma, from cross-sectional data. *Invest Ophthalmol Vis Sci.* 2008;49:66-76.
6. Sponsel WE, Groth SL, Satsangi N, Maddess T, Reilly MA. Refined data analysis provides clinical evidence for central nervous system control of chronic glaucomatous neurodegeneration. *Trans Vis Sci Technol.* 2014;3:1.
7. Lucas-Ruiz F, Galindo-Romero C, Rodríguez-Ramírez KT, Vidal-Sanz M, Agudo-Barriuso M. Neuronal death in the contralateral un-injured retina after unilateral axotomy: Role of microglial cells. *Int J Mol Sci.* 2019;20:5733.
8. Tribble JR, Kokkali E, Otmani A, et al. When is a control not a control? Reactive microglia occur throughout the control contralateral pathway of retinal ganglion cell projections in experimental glaucoma. *Transl Vis Sci Technol.* 2021;10:22.
9. Rojas B, Gallego BI, Ramírez AI, et al. Microglia in mouse retina contralateral to experimental glaucoma exhibit multiple signs of activation in all retinal layers. *J Neuroinflammation.* 2014;11:133.
10. Kezic JM, Chrysostomou V, Trounce IA, McMenamin PG, Crowston JG. Effect of anterior chamber cannulation and acute IOP elevation on retinal macrophages in the adult mouse. *Invest Ophthalmol Vis Sci.* 2013;54:3028-3036.
11. Gallego BI, Salazar JJ, de Hoz R, et al. IOP induces upregulation of GFAP and MHC-II and microglia reactivity in mice retina contralateral to experimental glaucoma. *J Neuroinflammation.* 2012;9:92.
12. González-Riquelme MJ, Galindo-Romero C, Lucas-Ruiz F, et al. Axonal injuries cast long shadows: Long term glial activation in injured and contralateral retinas after unilateral axotomy. *Int J Mol Sci.* 2021;22:8517.
13. Cooper ML, Pasini S, Lambert WS, et al. Redistribution of metabolic resources through astrocyte networks mitigates neurodegenerative stress. *Proc Natl Acad Sci U S A.* 2020;117:18810-18821.
14. Zhan Z, Wu Y, Liu Z, et al. Reduced dendritic spines in the visual cortex contralateral to the optic nerve crush eye in adult mice. *Invest Ophthalmol Vis Sci.* 2020;61:55.
15. Crish SD, Sappington RM, Inman DM, Horner PJ, Calkins DJ. Distal axonopathy with structural persistence in glaucomatous neurodegeneration. *Proc Natl Acad Sci U S A.* 2010;107:5196-5201.
16. Calkins DJ, Lambert WS, Formichella CR, McLaughlin WM, Sappington RM. The microbead occlusion model of ocular hypertension in mice. *Methods Mol Biol.* 2018;1695:23-39.
17. Pease ME, Hammond JC, Quigley HA. Manometric calibration and comparison of TonoLab and TonoPen tonometers in rats with experimental glaucoma and in Normal mice. *J Glaucoma.* 2006;15:512-519.
18. Reitsamer HA, Kiel JW, Harrison JM, Ransom NL, McKinnon SJ. Tonopen measurement of intraocular pressure in mice. *Exp Eye Res.* 2004;78:799-804.
19. Risner ML, Pasini S, McGrady NR, Calkins DJ. Bax contributes to retinal ganglion cell dendritic degeneration during glaucoma. *Mol Neurobiol.* 2022;59:1366-1380.
20. Ward NJ, Ho KW, Lambert WS, Weitlauf C, Calkins DJ. Absence of transient receptor potential vanilloid-1 accelerates stress-induced axonopathy in the optic projection. *J Neurosci.* 2014;34:3161-3170.
21. Risner ML, Pasini S, McGrady NR, et al. Neuroprotection by wld(S) depends on retinal ganglion cell type and age in glaucoma. *Mol Neurodegener.* 2021;16:36.
22. Risner ML, McGrady NR, Pasini S, Lambert WS, Calkins DJ. Elevated ocular pressure reduces voltage-gated sodium channel Nav1.2 protein expression in retinal ganglion cell axons. *Exp Eye Res.* 2020;190:107873.
23. Risner ML, McGrady NR, Boal AM, Pasini S, Calkins DJ. TRPV1 Supports axogenic enhanced excitability in response to neurodegenerative stress. *Front Cell Neurosci.* 2020;14:603419.
24. McGrady NR, Risner ML, Vest V, Calkins DJ. TRPV1 Tunes optic nerve axon excitability in glaucoma. *Front Physiol.* 2020;11:249.
25. Risner ML, Pasini S, Cooper ML, Lambert WS, Calkins DJ. Axogenic mechanism enhances retinal ganglion cell excitability during early progression in glaucoma. *Proc Natl Acad Sci U S A.* 2018;115:e2393-e2402.
26. Weitlauf C, Ward NJ, Lambert WS, et al. Short-term increases in transient receptor potential vanilloid-1 mediate stress-induced enhancement of neuronal excitation. *J Neurosci.* 2014;34:15369-15381.
27. Fischer RA, Risner ML, Roux AL, Wareham LK, Sappington RM. Impairment of membrane repolarization accompanies axon transport deficits in glaucoma. *Front Neurosci.* 2019;13:1139.
28. Baltan S, Inman DM, Danilov CA, Morrison RS, Calkins DJ, Horner PJ. Metabolic vulnerability disposes retinal ganglion cell axons to dysfunction in a model of glaucomatous degeneration. *J Neurosci.* 2010;30:5644-5652.
29. Caldwell JH, Schaller KL, Lasher RS, Peles E, Levinson SR. Sodium channel na(v)1.6 is localized at nodes of ranvier, dendrites, and synapses. *Proc Natl Acad Sci U S A.* 2000;97:5616-5620.
30. Hargus NJ, Nigam A, Bertram EH III, Patel MK. Evidence for a role of Nav1.6 in facilitating increases in neuronal hyperexcitability during epileptogenesis. *J Neurophysiol.* 2013;110:1144-1157.
31. Craner MJ, Lo AC, Black JA, Waxman SG. Abnormal sodium channel distribution in optic nerve axons in a model of inflammatory demyelination. *Brain.* 2003;126:1552-1561.
32. Boiko T, Rasband MN, Levinson SR, et al. Compact myelin dictates the differential targeting of two sodium channel isoforms in the same axon. *Neuron.* 2001;30:91-104.
33. Arancibia-Cárcamo IL, Ford MC, Cossell L, Ishida K, Tohyama K, Attwell D. Node of ranvier length as a potential regulator of myelinated axon conduction speed. *eLife.* 2017;6:e23329.
34. Berry RH, Qu J, John SW, Howell GR, Jakobs TC. Synapse loss and dendrite remodeling in a mouse model of glaucoma. *PLoS One.* 2015;10:e0144341.
35. Palop JJ, Mucke L. Network abnormalities and interneuron dysfunction in Alzheimer disease. *Nat Rev Neurosci.* 2016;17:777-792.
36. Fogarty MJ. Driven to decay: Excitability and synaptic abnormalities in amyotrophic lateral sclerosis. *Brain Res Bull.* 2018;140:318-333.
37. Trapp BD, Peterson J, Ransohoff RM, Rudick R, Mörk S, Bö L. Axonal transection in the lesions of multiple sclerosis. *N Engl J Med.* 1998;338:278-285.
38. Gastinger MJ, Kunselman AR, Conboy EE, Bronson SK, Barber AJ. Dendrite remodeling and other abnormalities in the retinal ganglion cells of Ins2 akita diabetic mice. *Invest Ophthalmol Vis Sci.* 2008;49:2635-2642.
39. Arancibia-Cárcamo IL, Attwell D. The node of ranvier in CNS pathology. *Acta Neuropathol.* 2014;128:161-175.
40. Rush AM, Dib-Hajj SD, Waxman SG. Electrophysiological properties of two axonal sodium channels, Nav1.2 and Nav1.6, expressed in mouse spinal sensory neurones. *J Physiol.* 2005;564:803-815.
41. Rasband MN, Peles E, Trimmer JS, Levinson SR, Lux SE, Shrager P. Dependence of nodal sodium channel clustering on paranodal axoglial contact in the developing CNS. *J Neurosci.* 1999;19:7516-7528.
42. Raman IM, Sprunger LK, Meisler MH, Bean BP. Altered subthreshold sodium currents and disrupted firing patterns in purkinje neurons of Scn8a mutant mice. *Neuron.* 1997;19:881-891.
43. Jurgens HA, Johnson RW. Dysregulated neuronal-microglial cross-talk during aging, stress and inflammation. *Exp Neurol.* 2012;233:40-48.

44. Chen W, Sheng J, Guo J, et al. Tumor necrosis factor- $\alpha$  enhances voltage-gated  $\text{Na}^+$  currents in primary culture of mouse cortical neurons. *J Neuroinflammation*. 2015;12:126-126.
45. Bleckert A, Schwartz GW, Turner MH, Rieke F, Wong RO. Visual space is represented by nonmatching topographies of distinct mouse retinal ganglion cell types. *Curr Biol*. 2014;24:310-315.
46. Beirowski B, Babetto E, Coleman MP, Martin KR. The WldS gene delays axonal but not somatic degeneration in a rat glaucoma model. *Eur J Neurosci*. 2008;28:1166-1179.
47. Beirowski B, Adalbert R, Wagner D, et al. The progressive nature of Wallerian degeneration in wild-type and slow Wallerian degeneration (WldS) nerves. *BMC Neurosci*. 2005;6:6.
48. Vidal-Sanz M, Galindo-Romero C, Valiente-Soriano FJ, et al. Shared and differential retinal responses against optic nerve injury and ocular hypertension. *Front Neurosci*. 2017;11:235.
49. Li L, Huang H, Fang F, Liu L, Sun Y, Hu Y. Longitudinal morphological and functional assessment of RGC neurodegeneration after optic nerve crush in mouse. *Front Cell Neurosci*. 2020;14:109.
50. Chen H, Wei X, Cho KS, et al. Optic neuropathy due to microbead-induced elevated intraocular pressure in the mouse. *Invest Ophthalmol Vis Sci*. 2010;52:36-44.
51. Marin MA, de Lima S, Gilbert HY, et al. Reassembly of excitable domains after CNS axon regeneration. *J Neurosci*. 2016;36:9148-9160.
52. Syc-Mazurek SB, Fernandes KA, Wilson MP, Shrager P, Libby RT. Together JUN and DDIT3 (CHOP) control retinal ganglion cell death after axonal injury. *Mol Neurodegener*. 2017;12:71.
53. Fernandes KA, Mitchell KL, Patel A, et al. Role of SARM1 and DR6 in retinal ganglion cell axonal and somal degeneration following axonal injury. *Exp Eye Res*. 2018;171:54-61.
54. Wang R, Chen Z, Wu J, et al. Preconditioning with carbon monoxide inhalation promotes retinal ganglion cell survival against optic nerve crush via inhibition of the apoptotic pathway. *Mol Med Rep*. 2018;17:1297-1304.
55. Smith MA, Plyler ES, Dengler-Criss CM, Meier J, Criss SD. Nodes of Ranvier in glaucoma. *Neuroscience*. 2018;390:104-118.
56. Bond WS, Hines-Beard J, GoldenMerry YPL, et al. Virus-mediated EpoR76E therapy slows optic nerve axonopathy in experimental glaucoma. *Mol Ther*. 2016;24:230-239.
57. Akopian A, Kumar S, Ramakrishnan H, et al. Targeting neuronal gap junctions in mouse retina offers neuroprotection in glaucoma. *J Clin Invest*. 2017;127:2647-2661.
58. Jnawali A, Lin X, Patel NB, Frishman LJ, Ostrin LA. Retinal ganglion cell ablation in guinea pigs. *Exp Eye Res*. 2021;202:108339.
59. Chrysostomou V, Crowston JG. The photopic negative response of the mouse electroretinogram: Reduction by acute elevation of intraocular pressure. *Invest Ophthalmol Vis Sci*. 2013;54:4691-4697.
60. Ou Y, Jo RE, Ullian EM, Wong RO, Della Santina L. Selective vulnerability of specific retinal ganglion cell types and synapses after transient ocular hypertension. *J Neurosci*. 2016;36:9240-9252.
61. Della Santina L, Inman DM, Lupien CB, Horner PJ, Wong RO. Differential progression of structural and functional alterations in distinct retinal ganglion cell types in a mouse model of glaucoma. *J Neurosci*. 2013;33:17444-17457.
62. Pang JJ, Gao F, Wu SM. Light-evoked excitatory and inhibitory synaptic inputs to ON and OFF alpha ganglion cells in the mouse retina. *J Neurosci*. 2003;23:6063-6073.
63. Schmidt TM, Alam NM, Chen S, et al. A role for melanopsin in alpha retinal ganglion cells and contrast detection. *Neuron*. 2014;82:781-788.
64. Duan X, Qiao M, Bei F, Kim I-J, He Z, Sanes JR. Subtype-specific regeneration of retinal ganglion cells following axotomy: Effects of osteopontin and mTOR signaling. *Neuron*. 2015;85:1244-1256.
65. Tran NM, Shekhar K, Whitney IE, et al. Single-cell profiles of retinal ganglion cells differing in resilience to injury reveal neuroprotective genes. *Neuron*. 2019;104:1039-1055.e1012.
66. La Morgia C, Ross-Cisneros FN, Sadun AA, et al. Melanopsin retinal ganglion cells are resistant to neurodegeneration in mitochondrial optic neuropathies. *Brain*. 2010;133:2426-2438.
67. El-Danaf RN, Huberman AD. Characteristic patterns of dendritic remodeling in early-stage glaucoma: Evidence from genetically identified retinal ganglion cell types. *J Neurosci*. 2015;35:2329-2343.
68. Tao X, Sabharwal J, Wu SM, Frankfort BJ. Intraocular pressure elevation compromises retinal ganglion cell light adaptation. *Invest Ophthalmol Vis Sci*. 2020;61:15.
69. Yang N, Young BK, Wang P, Tian N. The susceptibility of retinal ganglion cells to optic nerve injury is type specific. *Cells*. 2020;9:677.